
Few-shot Image Generation via Adaptation-Aware Kernel Modulation

Yunqing Zhao*

yunqing_zhao@mymail.sutd.edu.sg

Keshigeyan Chandrasegaran*

keshigeyan@sutd.edu.sg

Milad Abdollahzadeh*

milad_abdollahzadeh@sutd.edu.sg

Ngai-Man Cheung†

ngaiman_cheung@sutd.edu.sg

Singapore University of Technology and Design (SUTD)

Abstract

Few-shot image generation (FSIG) aims to learn to generate new and diverse samples given an extremely limited number of samples from a domain, *e.g.*, 10 training samples. Recent work has addressed the problem using transfer learning approach, leveraging a GAN pretrained on a large-scale source domain dataset and adapting that model to the target domain based on very limited target domain samples. Central to recent FSIG methods are *knowledge preserving criteria*, which aim to select a subset of source model’s knowledge to be preserved into the adapted model. However, a *major limitation* of existing methods is that their knowledge preserving criteria consider *only source domain/source task*, and they fail to consider *target domain/adaptation task* in selecting source model’s knowledge, casting doubt on their suitability for setups of different *proximity* between source and target domain. **Our work** makes two contributions. As our first contribution, we revisit recent FSIG works and their experiments. Our important finding is that, under setups which assumption of close proximity between source and target domains is relaxed, existing state-of-the-art (SOTA) methods which consider only source domain in knowledge preserving perform *no better* than a baseline fine-tuning method. To address the limitation of existing methods, as our second contribution, we propose *Adaptation-Aware kernel Modulation* (AdAM) to address general FSIG of different source-target domain proximity. Extensive experimental results show that the proposed method consistently achieves SOTA performance across source/target domains of different proximity, including challenging setups when source and target domains are more apart. Project Page: <https://yunqing-me.github.io/AdAM/>

1 Introduction

Generative Adversarial Networks (GANs) [1–3] have been applied to a range of important applications including image generation [4, 3, 5], image-to-image translation [6, 7], image editing [8, 9], anomaly detection [10], and data augmentation [11, 12]. However, a critical issue is that these GANs often require large-scale datasets and computationally expensive resources to achieve good performance. For example, StyleGAN [4] is trained on Flickr-Faces-HQ (FFHQ) [4] that contains 70,000 images. However, in many practical applications only a few samples are available (*e.g.*, photos of rare animal species / skin diseases). Training a generative model is problematic in this low-data regime, where the generator often suffers from mode collapse or blurred generated images [13–15]. To address this, *few-shot image generation* (FSIG) studies the possibility of generating sufficiently diverse and high

*Equal Contribution †Corresponding Author

Table 1: Transfer learning for few-shot image generation: Various criteria are proposed to *augment* baseline transfer learning to preserve subset of source model’s knowledge into the adapted model.

Method	Knowledge preserving criteria	Source domain/task aware	Target domain/adaptation aware
TGAN [16]	Not available	–	–
FreezeD [17]	Preservation of lower layers of the discriminator pre-trained on the <i>source</i> domain.	✓	✗
EWC [18]	Preservation of weights important to the <i>source</i> generative model pre-trained on the <i>source</i> domain.	✓	✗
CDC [14]	Preservation of pairwise distances of generated images by the <i>source</i> generative model pre-trained on the <i>source</i> domain.	✓	✗
DCL [19]	Preservation of multilevel semantic diversity of the generated images by the <i>source</i> generative model pre-trained on the <i>source</i> domain.	✓	✗
AdAM (Our work)	Preservation of kernels important in <i>adaptation</i> of source model to <i>target</i> .	✓	✓

quality images, given very limited training data (*e.g.*, 10 samples). FSIG also attracts an increasing interest for some downstream tasks, *e.g.*, few-shot classification [12].

FSIG with Transfer Learning. Recent works in FSIG are based on transfer learning approach [20] *i.e.*, leveraging the prior knowledge of a GAN pretrained on a large-scale, diverse source dataset (*e.g.*, FFHQ [4] or ImageNet [21]) and adapting it to a target domain with very limited samples (*e.g.*, face paintings [22]). As only very limited samples are provided to define the underlying distribution, standard fine-tuning of a pre-trained GAN suffers from mode collapse: the adapted model can only generate samples closely resembling the given few shot target samples [16, 14]. Therefore, recent works [18, 14, 19] have proposed to *augment* standard fine-tuning with different criteria to carefully preserve subset of source model’s knowledge into the adapted model. Various criteria has been proposed (Table 1), and these *knowledge preserving criteria* have been central in recent FSIG research. In general, these criteria aim to preserve subset of source model’s knowledge which is deemed to be useful for target-domain sample generation, *e.g.*, improving the diversity of target sample generation.

Research Gaps. One major limitation of existing methods is that they consider *only* source domain in preserving subset of source model’s knowledge into the adapted model. In particular, these methods *fail to consider* target domain/adaptation task in selection of source model’s knowledge (Table 1). For example, EWC [18] applies Fisher Information [23] to select important weights entirely based on the pretrained *source* model, and it aims to preserve these selected weights regardless of the target domain in adaptation. Similar to EWC [18], CDC [14] proposes an additional constraint to preserve pairwise distances of generated images by the *source* model, and there is no consideration of target domain/adaptation. These *target/adaptation-agnostic* knowledge preserving criteria in recent works raise question regarding their suitability in different source/target domain setups. It should be noted that existing FSIG works (under very limited target samples) focus largely on setups where source and target domains are in *close proximity* (semantically) *e.g.*, Human faces (FFHQ)→Baby faces [14, 19], or Cars→Abandoned Cars [14, 19]. It is unclear about their performance when source/target domains are more apart (*e.g.*, Human faces (FFHQ) → Animal faces [5]).

Contributions. In this paper we take an important step to address these research gaps for FSIG. Specifically, our work makes two contributions. **As our first contribution**, we revisit existing state-of-the-art (SOTA) algorithms and their experiments. Importantly, we observe that when the close proximity assumption is relaxed in experiment setups and source/target domains are more apart, existing SOTA methods perform *no better* than a baseline fine-tuning method. Our observation suggests that recent methods considering only source domain/source task in knowledge preserving may not be suitable for *general* FSIG when source and target domains are more apart. To validate our claims, we introduce additional experiments with different source/target domains, analyze their proximity qualitatively and quantitatively, and examine existing methods under a unified framework.

Informed by our analysis, **as our second contribution**, we propose an *adaptation-aware kernel modulation* approach to address general FSIG of different source/target domain proximity. In marked contrast to existing works which preserve knowledge important to *source* task, our method aims to preserve subset of source model’s knowledge that are important to the *target* domain and the *adaptation* task. More specifically, we propose an *importance probing* algorithm to identify kernels which encode important knowledge for adaptation to the target domain. Then, we preserve the knowledge of these kernels using a parameter-efficient *rank-constrained kernel modulation*.

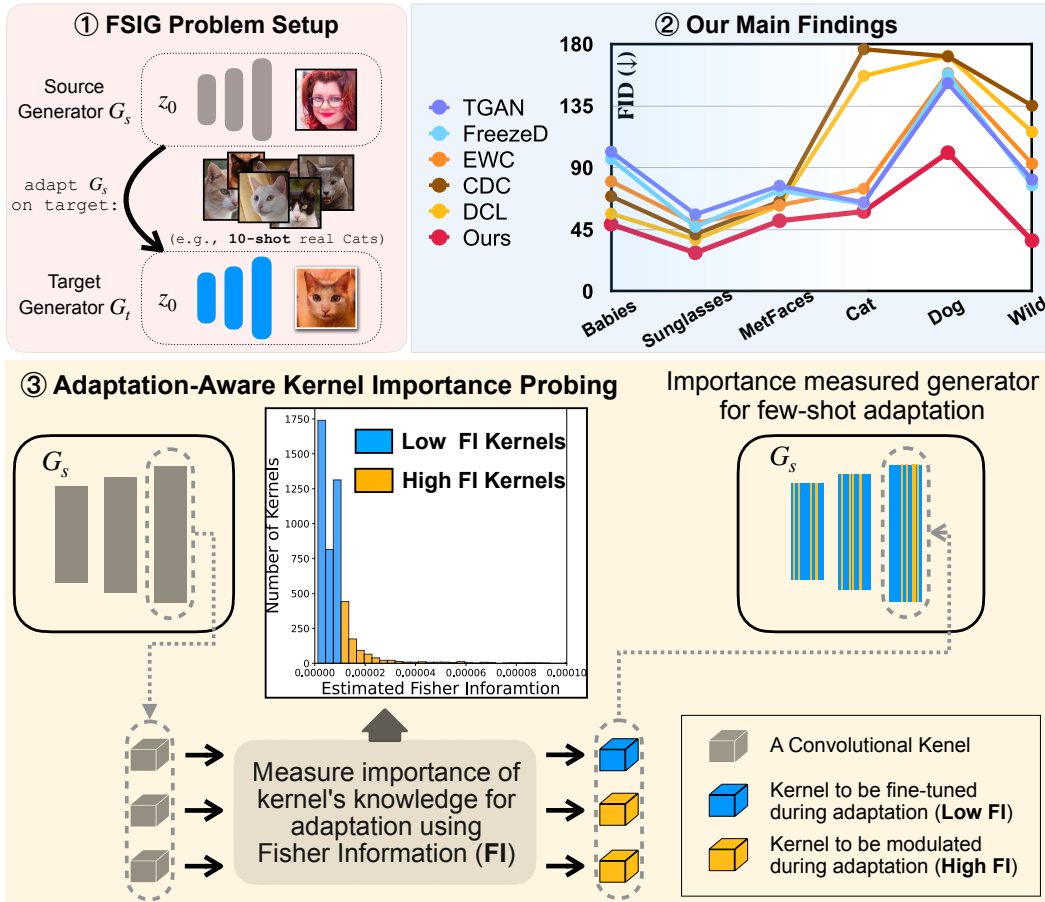


Figure 1: *Overview and our contributions.* ①: We consider the problem of FSIG with Transfer Learning using very limited target samples (*i.e.* 10-shot). ②: Our work makes two contributions, • We discover that when the close proximity assumption between source-target domain is relaxed, SOTA FSIG methods (EWC [18], CDC [14], DCL [19]) which consider only source domain/source task in knowledge preserving perform no better than a baseline fine-tuning method (TGAN [16]) (Sec 3). • We propose a novel adaptation-aware kernel modulation for FSIG that achieves SOTA performance across source / target domains with different proximity (Sec 4). ③ Schematic diagram of our proposed Importance Probing Mechanism: We measure the importance of each kernel for the target domain after probing and preserve source domain knowledge that is important for target domain adaptation (Sec 4). The same operations are applied to discriminator.

We conduct extensive experiments to show that our proposed method consistently achieves SOTA performance across source/target domains of different proximity, including challenging setups when source/target domains are more apart. Our main contributions are summarized as follows:

- We revisit existing FSIG methods and experiment setups. Our study uncovers issues with existing methods when applied to source/target domains of different proximity.
- We propose Adaptation-Aware kernel Modulation (AdAM) for FSIG. Our method consistently achieves SOTA performance both visually and quantitatively across source/target domains with different proximity.

2 Related Work

Few-shot image generation. Conventional few-shot learning [24–26] aims at learning a discriminative classifier for classification [27–30], segmentation [31, 32] or detection [33–35] tasks. Differently, few-shot image generation (FSIG) [14, 18, 19] aims at learning a generator for new and diverse samples given extremely limited samples (*e.g.*, 10 shots). Transfer learning has been applied to FSIG. For example, Transferring GAN [16] (TGAN) applies simple GAN loss [1] to fine-tune all parameters

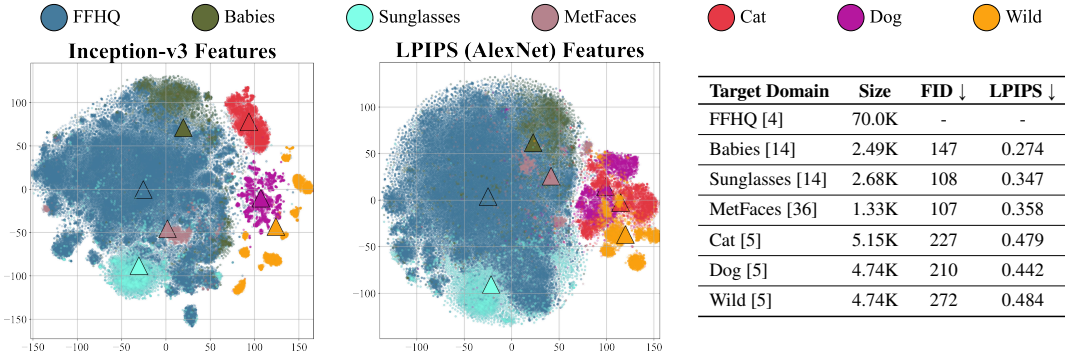


Figure 2: *Qualitative / Quantitative analysis of source-target domain proximity*: We use FFHQ [3] as the source domain. We show source-target domain proximity qualitatively by visualizing Inception-v3 (Left) [37] and LPIPS (Middle) [38] – using AlexNet [39] backbone – features, and quantitatively using FID / LPIPS metrics (Right). For feature visualization, we use t-SNE [40] and show centroids (\triangle) for all domains. FID / LPIPS is measured with respect to FFHQ. There are two important observations: ① Common target domains used in existing FSIG works (Babies, Sunglasses, MetFaces) are notably proximal to the source domain (FFHQ). This can be observed from the feature visualization and verified by FID / LPIPS measurements. ② We clearly show using feature visualizations and FID / LPIPS measurements that additional setups – Cat [5], Dog [5] and Wild [5] – represent target domains that are distant from the source domain (FFHQ). We remark that large FID values in this analysis are reasonable due to the distance between the source (FFHQ) and different target domains as observed from centroid distance / feature variance. The effect of limited sample size (target domains) for FID / LPIPS measurements are minimal and we include rich supportive studies in Supplementary. Additional experiments and source/target setups in Supplementary to further support our analysis.

of both the generator and the discriminator. **FreezeD** [17] fixes a few high-resolution discriminator layers during fine-tuning. To augment and improve simple fine-tuning, more recent works have focused on preserving specific knowledge from the source models. Elastic weight consolidation (**EWC**) [18] identifies important weights for the *source* model and tries to preserve these weights. Cross-domain Correspondence (**CDC**) [14] preserves pair-wise distance of generated images from the source model to alleviate mode collapse. Dual Contrastive Learning (**DCL**) [19] applies mutual information maximization to preserve multi-level diversity of the generated images by the source model. In this work, we observe that these SOTA methods perform poorly when source and target domains are more apart. Therefore, their proposed source knowledge preservation criteria *may not* be generalizable. Based on our analysis, we propose an adaptation-aware knowledge selection which is more *generalizable* for source/target domains with different proximity.

3 Revisiting FSIG through the Lens of Source–Target Domain Proximity

In this section, we revisit existing FSIG methods (10-shot) [16–18, 14, 19] through the lens of source-target domain proximity. Specifically, we scrutinize the experimental setups of existing FSIG methods and observe that SOTA [18, 14, 19] largely focus on adapting to target domains that are (semantically) proximal to the source domain: Human Faces (FFHQ) \rightarrow Baby Faces; Human Faces (FFHQ) \rightarrow Sunglasses; Cars \rightarrow Abandoned Cars; Church \rightarrow Haunted Houses [18, 14, 19]. This raises the question as to whether existing source-target domain setups sufficiently represent *general* FSIG scenarios. Particularly, real-world FSIG applications may not contain target domains that are always proximal to the source domain (*e.g.*, Human Faces (FFHQ) \rightarrow Animal Faces). Motivated by this, we conduct an in-depth qualitative and quantitative analysis on source-target domain proximity where we introduce target domains that are distant from the source domain (Sec 3.1). Our analysis uncovers an important finding: **Under our additional setups where the assumption of close proximity between source and target domain is relaxed, existing SOTA FSIG methods [18, 14, 19] which consider only source domain/source task in knowledge preserving perform *no better* than a baseline fine-tuning method.** We show this is due to the strong focus of existing SOTA methods in preserving source domain knowledge, thereby not being able to adapt well to distant target domains (Sec 3.2).

3.1 Source–Target Domain Proximity Analysis

Introducing target domains with varying degrees of proximity to the source domain. In this section, we formally introduce source-target domain proximity with in-depth analysis to scrutinize existing FSIG methods under different degrees of source-target domain proximity. Following prior FSIG works [16–18, 14, 19], we use FFHQ [3] as the source domain in this analysis. We remark that existing works largely consider different types of human faces as target domain (*i.e.*: Babies [14], Sunglasses [14], MetFaces [36]), To relax the close proximity assumption and study *general* FSIG problems, we introduce more distant target domains namely Cat, Dog and Wild (from AFHQ [5], consisting of 15,000 high-quality animal face images at 512×512 resolution) for our analysis.

Characterizing source-target domain proximity. Given the wide success of deep neural network features in representing meaningful semantic concepts [41–43], we visualize Inception-v3 [37] and LPIPS [38] features for source and target domains to qualitatively characterize domain proximity. Further, we use FID [44] and LPIPS distance to quantitatively characterize source-target domain proximity. We remark that FID involves distribution estimation (first, second order moments) [44] and LPIPS computes pairwise distances (learned embeddings) [38] between source / target domains.

Analysis. Feature visualization and FID/ LPIPS measurement results are shown in Figure 2. Our results both qualitatively (columns 1, 2) and quantitatively (column 3) show that target domains used in existing works (Babies [3], Sunglasses [3], MetFaces [36]) are notably proximal to the source domain (FFHQ), and our additionally introduced target domains (Dog, Cat and Wild [5]) are distant from the source domain thereby relaxing the close proximity assumption in existing FSIG works.

3.2 FSIG methods under Relaxation of Close Domain Proximity Assumption

Motivated by our analysis in Section 3.1, we investigate the performance of existing FSIG methods [16–18, 14, 19] by relaxing the close proximity assumption between source and target domains. We investigate the performance of these FSIG methods across target domains of different proximity to the source domain, which includes our additionally introduced target domains: Dog, Cat and Wild. The FID results for FFHQ \rightarrow Cat are: TGAN (simple fine-tuning) [16]: 64.68, EWC [18]: 74.61, CDC [14]: 176.21, DCL [19]: 156.82. Full results can be found in Table 2. We emphasize that our investigation uncovers an important finding: *Under setups which the assumption of close proximity between source and target domain is relaxed (Dog, Cat, Wild), existing SOTA FSIG methods [18, 14, 19] perform no better than a baseline method [16]. This can be consistently observed in Table 2.*

This finding is critical as it exposes a serious drawback of SOTA FSIG methods [18, 14, 19] when close domain proximity (between source and target) assumption is relaxed. We further analyse generated images from SOTA FSIG methods and observe that these methods are unable to adapt well to distant target domains due to *only considering source domain / task in knowledge preservation*. This can be clearly observed from Figure 3. We remark that TGAN (simple baseline) [16] also suffers from severe mode collapse. Given that our investigation uncovers an important problem in SOTA FSIG methods, we tackle this problem in Sec 4. Figure 3 (last row) shows a glimpse of our proposed method.

4 Adaptation-Aware Kernel Modulation

We focus on this question: “Given a pretrained GAN on a source domain \mathcal{D}_s , and a few-samples from a target domain \mathcal{D}_t , which part of the source model’s knowledge should be preserved, and which part should be updated, during the adaptation from \mathcal{D}_s to \mathcal{D}_t ?” In contrast to

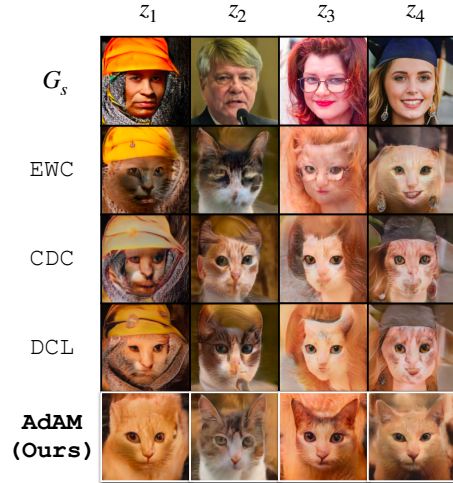


Figure 3: G_s is the source generator (FFHQ). Adapting from the source domain (FFHQ) to a distant target domain (Cat) using SOTA FSIG methods EWC [18], CDC [14], DCL [19] (rows 2, 3, 4) results in observable knowledge transfer that is not useful to the target domain. *i.e.*: Source task knowledge such as Caps (z_1, z_4), Hair styles/color – brown (z_2), red-hair (z_3), Eye glasses (z_3) from FFHQ are transferred to Cats during adaptation which is not appropriate. Our method (last row) can alleviate these issues.

Algorithm 1: Few-Shot Image Generation via Adaptation-Aware Kernel Modulation (AdAM)

Require: Pre-trained GAN: G_s and D_s , $iter_{probe}$, $iter_{adapt}$, threshold quantile t , learning rate α

Importance Probing:

```
1 Freeze all kernels  $\{\mathbf{W}_i\}_{i=1}^N$  in pre-trained networks  $G_s$ , and  $D_s$ 
2 Randomly initialize a modulation matrix  $\mathbf{M}_i$  for each kernel  $\mathbf{W}_i$ 
3 for  $k = 0, k++$ , while  $k < iter_{probe}$  do
4   | Perform kernel modulation for all kernels using Eqn.1 to obtain modulated weights  $\hat{\mathbf{W}}$ 
5   | Update  $\mathbf{M} \leftarrow \mathbf{M} - \alpha \nabla_{\mathbf{M}} \mathcal{L}(G(z); \hat{\mathbf{W}})$  /* lightweight, i.e.,  $iter_{probe} \ll iter_{adapt}$  */
6 end
7 Measure importance of each kernel  $\mathbf{W}_i$  by computing FI for the corresponding  $\mathbf{M}_i$  using Eqn.3
8 Compute the index set  $\mathcal{A}$  of important kernels using quantile  $t$  of FI values as threshold
Main Adaptation:
9 if  $j \in \mathcal{A}$  then
10  | Initialize the kernel by  $\mathbf{W}_j$  and freeze the kernel, randomly initialize  $\mathbf{M}_j$ 
11 else
12  | Initialize the kernel by  $\mathbf{W}_j$ 
13 end
14 for  $k = 0, k++$ , while  $k < iter_{adapt}$  do
15  | if  $j \in \mathcal{A}$  then
16  |   | Modulate kernel using Eqn.1 to obtain modulated weights  $\hat{\mathbf{W}}_j$ 
17  |   | Update  $\mathbf{M}_j \leftarrow \mathbf{M}_j - \alpha \nabla_{\mathbf{M}_j} \mathcal{L}(G(z); \hat{\mathbf{W}}_j)$ 
18  |   else
19  |   | Update  $\mathbf{W}_j \leftarrow \mathbf{W}_j - \alpha \nabla_{\mathbf{W}_j} \mathcal{L}(G(z); \hat{\mathbf{W}}_j)$ 
20  |   end
21 end
```

SOTA FSIG methods [18, 14, 19], we propose an adaptation-aware FSIG that also considers the target domain / adaptation task in deciding which part of the source model’s knowledge to be preserved. In a CNN, each *kernel* is responsible for a specific part of knowledge (e.g., pattern or texture). Similar behaviour is also observed for both generator [45] and discriminator [46] in GANs. Therefore, in this work, we make this knowledge preservation decision at the kernel level, *i.e.*, **casting the knowledge preservation to a decision problem of whether a kernel is important when adapting from \mathcal{D}_s to \mathcal{D}_t .**

Our FSIG algorithm has two main steps: (i) a lightweight *importance probing* step, and (ii) *main adaptation* step. In the first step, *i.e.*, importance probing, we adapt the model using a parameter-efficient design to the target domain for a limited number of iterations, and during this adaptation, we measure the importance of each individual kernel for the *target domain*. The output of importance probing are decisions of importance / unimportance of individual kernels. Then, in the second step, *i.e.*, main adaptation, we preserve the knowledge of important kernels and update the knowledge of unimportant kernels. The overview of the proposed system is shown in Figure 1 and the pseudocode is shown in Algorithm 1.

Proposed Importance Probing for FSIG. Our intuition for the proposed importance probing is: “The source GAN kernels have different levels of importance for each target domain.” For example, different subsets of kernels could be important when adapting a pretrained GAN on FFHQ to Babies [14] compared to adapting the same pretrained GAN to Cat [5]. Therefore, we aim for a knowledge preservation criterion that is target domain/adaptation-aware (Table 1). In order to achieve adaptation-awareness, we propose a light-weight importance probing algorithm which considers adaptation from source to target domain. There are two important design considerations: probing under (i) extremely limited number of target data and (ii) low computation overhead.

As discussed, in this *importance probing* step, we adapt the source model to the target domain for a limited number of iterations and with a few available target samples. During this short adaptation step, we measure the importance of kernel for the adaptation task. To measure the importance, we use Fisher information (FI) which gives the *informative knowledge* of that kernel in handling adaptation

task [47]. Then, based on FI measurement, we classify kernels into important / unimportant. These kernel-level importance decisions are then used in the next step, *i.e.*, main adaptation.

In the main adaptation step, we propose to apply *kernel modulation* to achieve restrained update for the important kernels, and *simple fine-tuning* for the unimportant kernels. As will be discussed, the modulation is rank-constrained and has restricted degree-of-freedom; therefore, it is capable to preserve knowledge of the important kernels. On the other hand, simple fine-tuning has large degree-of-freedom for updating knowledge of the unimportant kernels. Furthermore, the rank-constrained kernel modulation is parameter-efficient. Therefore, we also apply this rank-constrained kernel modulation *in the probing step* to determine the importance of kernels.

Kernel Modulation. The kernel modulation is used in the main adaptation step to preserve knowledge of important kernels into the adapted model. Furthermore, it is also used in the probing step as a parameter-efficient technique to determine importance of kernels. Specifically, we apply Kernel Modulation (KML) which is proposed very recently [29]. In [29], KML is proposed for multimodal few-shot *classification* (FSC). In particular, in [29], KML has been found to be effective for knowledge transfer between different *classification* tasks of different modes under few-shot constraint. Therefore, in our work, we apply KML for knowledge transfer between different *generation* tasks of different domains under limited target domain samples.

Specifically, in each convolutional layer of a CNN, the i^{th} kernel of that layer $\mathbf{W}_i \in \mathbb{R}^{c_{in} \times k \times k}$ is convolved with the input feature $\mathbf{X} \in \mathbb{R}^{c_{in} \times h \times w}$ to the layer to produce the i^{th} output channel (feature map) $\mathbf{Y}_i \in \mathbb{R}^{h' \times w'}$, *i.e.*, $\mathbf{Y}_i = \mathbf{W}_i * \mathbf{X} + b_i$, where $b_i \in \mathbb{R}$ denotes the bias term. Then, KML [29] modulates \mathbf{W}_i by multiplying it with the modulation matrix $\mathbf{M}_i \in \mathbb{R}^{c_{in} \times k \times k}$ plus an all-ones matrix $\mathbf{J} \in \mathbb{R}^{c_{in} \times k \times k}$:

$$\hat{\mathbf{W}}_i = \mathbf{W}_i \odot (\mathbf{J} + \mathbf{M}_i) \quad (1)$$

where \odot denotes Hadamard multiplication. In Eqn. 1, using \mathbf{J} allows to learn the modulation matrix in a residual format. Therefore, the modulation weights are learned as perturbations around the pretrained kernels which helps to preserve source knowledge. The exact pretrained kernel can also be transferred to the target model if it is optimal. There are some important differences between discriminative version of KML in [29] and our version, please see Supplementary for details.

This baseline KML learns an individual modulation parameter for each coefficient of the kernel. Therefore, it could suffer from *parameter explosion* when using in recent GAN architectures (*e.g.*, more than 58M parameters in StyleGAN-V2 [3]¹). To address this issue, instead of learning the modulation matrix, we learn a *low-rank* version of it [29, 48]. More specifically, for a Conv layer within CNN, with a total number of d_{out} kernels to be modulated, instead of learning $\mathbf{M} = \{\mathbf{M}_i\}_{i=1}^{d_{out}}$, we learn two proxy vectors $\mathbf{m}_1 \in \mathbb{R}^{d_{out}}$, and $\mathbf{m}_2 \in \mathbb{R}^{(c_{in} \times k \times k)}$, and construct the modulation matrix using the outer product of these vectors, *i.e.*, $\mathbf{M} = \mathbf{m}_1 \otimes \mathbf{m}_2$. Furthermore, as we are using KML for adaptable knowledge preservation, we *freeze* the base kernel \mathbf{W}_i during adaptation. Therefore, trainable parameters are $\mathbf{m}_1, \mathbf{m}_2$. This reduces the number of trainable parameters significantly, and has better performance on restraining the update of important kernels (see Supplementary). As it will be discussed later, the value of d_{out} equals to the total number of kernels in a layer (c_{out}) during probing, and for main adaptation, it is determined by the output of our probing method ($d_{out} \leq c_{out}$).

Importance Measurement. Recall our FSIG has two main steps: (i) importance probing step (Lines 1-8 in Algorithm 1), and (ii) main adaptation step (Lines 9-21 in Algorithm 1). In probing, we also apply KML as a parameter-efficient technique to determine importance of individual kernels. In particular, for probing, we apply KML to all kernels (in both generator and discriminator) to identify which of the *modulated* kernels are important for the adaptation task. To measure the importance of the modulated kernels, we apply Fisher information (FI) to the modulation parameters. In our FSIG setup, for a modulated GAN with parameters Θ , Fisher information \mathcal{F} can be computed as:

$$\mathcal{F}(\Theta) = \mathbb{E} \left[- \frac{\partial^2}{\partial \Theta^2} \mathcal{L}(x|\Theta) \right] \quad (2)$$

where $\mathcal{L}(x|\Theta)$ is the binary cross-entropy loss computed using the output of the discriminator, and x includes few-shot target samples, and fake samples generated by GAN. Then, FI for a modulation matrix $\mathcal{F}(\mathbf{M}_i)$ can be computed by averaging over FI values of parameters within that matrix. As we are using the low-rank estimation to construct the modulation matrix, we can estimate $\mathcal{F}(\mathbf{M}_i)$ by FI

¹<https://github.com/rosinality/stylegan2-pytorch>

Table 2: FSIG (10-shot) results: We report FID scores (\downarrow) of our proposed *adaptation-aware* FSIG and compare with existing FSIG methods. We emphasize that Cat, Dog and Wild target domains are additional experiments included in this work. (Sec 3.1). Our experiment results show two important findings: **1)** Under setups which assumption of close proximity between source and target domains is relaxed (Cat, Dog, Wild), SOTA FSIG methods – EWC, CDC, DCL – which consider only source domain in knowledge preserving perform *no better* than a baseline fine-tuning method (TGAN). **2)** Our proposed adaptation-aware FSIG achieves SOTA performance in *all* target domains due to preserving source domain knowledge that is important for few-shot target domain adaptation. We generate 5,000 images using the adapted generator to evaluate FID on the whole target domain. We also report the corresponding KID, Intra-LPIPS and standard deviations in Supplementary.

Target Domain	Babies [14]	Sunglasses [14]	MetFaces [36]	AFHQ-Cat [5]	AFHQ-Dog [5]	AFHQ-Wild [5]
TGAN [16]	101.58	55.97	76.81	64.68	151.46	81.30
TGAN+ADA [36]	97.91	53.64	75.82	80.16	162.63	81.55
FreezeD [17]	96.25	46.95	73.33	63.60	157.98	77.18
EWC [18]	79.93	49.41	62.67	74.61	158.78	92.83
CDC [14]	69.13	41.45	65.45	176.21	170.95	135.13
DCL [19]	56.48	37.66	62.35	156.82	171.42	115.93
AdAM (Ours)	48.83	28.03	51.34	58.07	100.91	36.87

values of the proxy vectors. In particular, considering the outer product in low-rank approximation, we have $\mathbf{M}_i = \text{reshape}([\mathbf{m}_1^i \mathbf{m}_2^1, \dots, \mathbf{m}_1^i \mathbf{m}_2^{(c_{in} \times k \times k)}])$, where $|\mathbf{m}_2| = c_{in} \times k \times k$. Then we use the unweighted average of FI for parameters of \mathbf{m}_1 and \mathbf{m}_2 , proportional to their occurrence frequency in calculation of \mathbf{M}_i , as an estimate of $\mathcal{F}(\mathbf{M}_i)$ (details in Supplementary):

$$\hat{\mathcal{F}}(\mathbf{M}_i) = \mathcal{F}(\mathbf{m}_1^i) + \frac{1}{|\mathbf{m}_2|} \sum_{j=1}^{|\mathbf{m}_2|} \mathcal{F}(\mathbf{m}_2^j) \quad (3)$$

After calculating $\hat{\mathcal{F}}(\mathbf{M}_i)$ for all modulation matrices in both generator and discriminator, we use the $t\%$ quantile of these values as a threshold (separately for generator and discriminator) to decide whether modulation of a kernel is important or unimportant for adaptation to the target domain. If the modulation of a kernel is determined to be important (during probing), the kernel is modulated using KML during main adaptation step; otherwise, the kernel is updated using simple fine-tuning during main adaptation. In all setups, we perform probing for 500 iterations. We remark that in probing only modulation parameters \mathbf{m}_1 , \mathbf{m}_2 are trainable, and FI is only computed on them, therefore the probing is a very lightweight step and can be performed with minimal overhead (details in Supplementary). The output of probing step are the decisions to apply kernel modulation or simple fine-tuning on individual kernels. Then, based on these decisions, the main adaptation is performed. The proposed FSIG scheme is summarized in Algorithm 1.

5 Empirical Studies

5.1 Experiments / Results

Experiment Details. For fair comparison, we strictly follow prior works [16–18, 14, 19] in the choice of GAN architecture, source-target adaptation setups and hyper-parameters. We use StyleGAN-V2 [3] as the GAN architecture and FFHQ as the source domain. Our experiments include setups with different source-target proximity: Babies/Sunglasses [14], MetFaces [36] and Cat/Dog/Wild (AFHQ) [5] (See Sec. 3). Adaptation is performed with 256 x 256 resolution and batch size 4 on a Tesla V100 GPU. We apply importance probing and modulation on base kernels of both generator and discriminator. We focus on 10-shot target adaptation setup in the main paper.

Qualitative Results. We show generated images with our proposed AdAM along Baseline [16, 17] and SOTA FSIG methods [18, 14, 19] for two target domains, Babies and Cat with different degrees of proximity to FFHQ, before and after adaptation. The results are shown in Figure 4 top and bottom, respectively. By preserving source domain knowledge that is important for target domain, our proposed adaptation-aware FSIG method can generate substantially high quality images with

		FID (\downarrow)	Intra-LPIPS (\uparrow)
10-Shot Real Babies	TGAN	101.58	0.517
	TGAN + ADA	97.91	0.511
	FreezeD	96.25	0.518
	EWC	79.93	0.521
	CDC	69.13	0.578
	DCL	56.48	0.580
	AdAM (Ours)	48.83	0.590
G_s (Pretrained)			
10-Shot Real Cats	TGAN	64.68	0.490
	TGAN + ADA	80.16	0.513
	FreezeD	63.60	0.492
	EWC	74.61	0.587
	CDC	176.21	0.629
	DCL	156.82	0.616
	AdAM (Ours)	58.07	0.557
G_s (Pretrained)			

Figure 4: Qualitative and quantitative comparison of 10-shot image generation with different FSIG methods. Images of each column are from the same noise input. **Left:** 10 real target images for few-shot adaptation. **Middle, Right:** For target domain with close proximity (*e.g.* Babies, top), our method can generate high quality images with more refined details and diversity knowledge, achieving best FID and Intra-LPIPS score. For target domain which is distant (*e.g.*, Cat, bottom), TGAN/FreezeD overfit to the 10-shot samples and others fail. In contrast, our method preserves meaningful semantic features at different levels (*e.g.*, posture and color) from source, achieving a good trade off between quality and diversity. In particular, our Intra-LPIPS approaches that of EWC, while our generated images have much better quality qualitatively and quantitatively.

high diversity for both Babies and Cat domains. We also include FID [44] and Intra-LPIPS [14] (for measuring diversity) to quantitatively show that our proposed method outperforms SOTA FSIG methods [18, 14, 19]. We show more generated samples in Supplementary.

Quantitative Results. We show complete FID (\downarrow) scores in Table 2. Our proposed AdAM for FSIG achieves SOTA results across all target domains of varying proximity to the source (FFHQ). We emphasize that it is achieved by preserving source domain knowledge that is important for target domain adaptation (Sec 4). We also report Intra-LPIPS (\uparrow) as an indicator of diversity, as Figure 4.

5.2 Analysis

Ablation study of Importance Probing. The goal of importance probing (denoted as “IP”) is to identify kernels that are important for *few-shot target adaptation* as shown in Figure 5 (Top). To justify the effectiveness of our design choice, we perform an ablation study that discards the IP stage and regard all kernels as *equally important* for target adaptation. Therefore, we simply modulate all

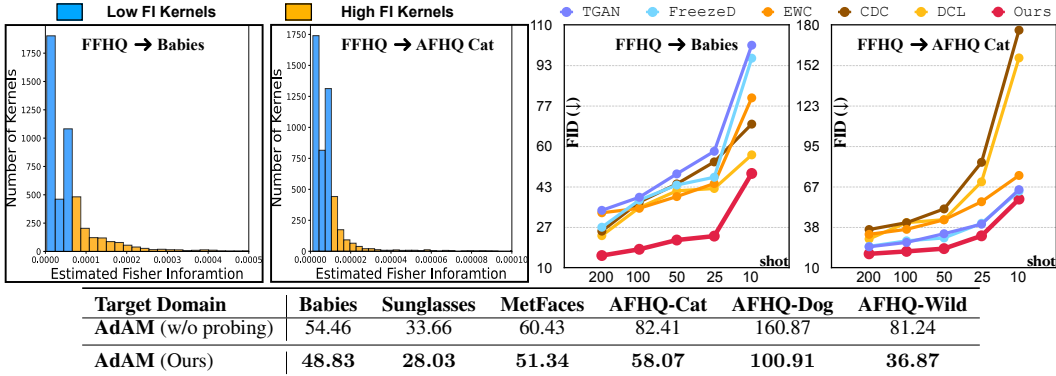


Figure 5: **(Top Left)** Our proposed IP identifies and preserves source kernels important (high FI) for target adaptation. **(Bottom)** FID score on different datasets. We validate the effectiveness of IP by modulating all kernels without IP. On the other hand, if we fine-tune all parameters without IP and modulation (TGAN), it suffers mode collapse (Table 2 and Figure 4). **(Top Right)** We evaluate the performance of different number of shots (10, 25, 50, 100, 200) on Babies and AFHQ-Cat. We show that our method consistently outperforms other FSIG methods in all setups. In Supplementary, we also show the generated images given different number of shots on more target domains.

kernels *without any knowledge selection*. As one can observe from Figure 5 (Bottom), knowledge selection plays a vital role in adaptation performance. Specifically, the significance of knowledge preservation is more evident when the target domains are distant from the source domain.

Number of target samples (shots). The number of target domain training samples is an important factor that can impact the FSIG performance. In general, more target domain samples can allow better estimation of target distribution. We study the efficacy of our proposed method under different number of target domain samples. The results are shown in Figure 5, and we show that our proposed adaptation-aware FSIG method consistently outperforms existing methods in all setups.

6 Discussion

Conclusion. Focusing on FSIG, we make two contributions. First, we revisit current SOTA methods and their experiments. We discover that SOTA methods perform poorly in setups when source and target domains are more distant, as existing methods only consider source domain/task for knowledge preservation. Second, we propose a new FSIG method which is target/adaptation-aware (AdAM). Our proposed method outperforms previous work across all setups of different source-target domain proximity. We include extended experiments and analysis in Supplementary.

Broader Impact. Our work makes contribution to generation of synthetic data in applications where sample collection is challenging, *e.g.*, photos of rare animal species. This is an important contribution to many data-centric applications. Furthermore, transfer learning of generative models using a few data sample enables data and computation-efficient model development. Our work has positive impact on environmental sustainability and reduction of greenhouse gas emission. While our work targets generative applications with limited-data, it parallelly raises concerns regarding such methods being used for malicious purposes. Given the recent success of forensic detectors [49–52], we conduct a simple study using Color-Robust forensic detector proposed in [49] on our Babies and Cat datasets. We observe that the model achieves 99.8% and 99.9% average precision (AP) respectively showing that AdAM samples can be successfully detected. We also remark that our work presents opportunities for improving knowledge transfer methods [53–56] in a broader context.

Limitations. While our experiments are extensive compared to previous works, in practical applications, there are many possible target domains which cannot be included in our experiments. However, as our method is target/adaptation aware, we believe our method can generalize better than existing SOTA which are target-agnostic.

References

- [1] Ian Goodfellow, Jean Pouget-Abadie, Mehdi Mirza, Bing Xu, David Warde-Farley, Sherjil Ozair, Aaron Courville, and Yoshua Bengio. Generative adversarial nets. *Advances in neural information processing systems*, 27, 2014.
- [2] Andrew Brock, Jeff Donahue, and Karen Simonyan. Large scale gan training for high fidelity natural image synthesis. *International Conference on Learning Representations*, 2018.
- [3] Tero Karras, Samuli Laine, Miika Aittala, Janne Hellsten, Jaakko Lehtinen, and Timo Aila. Analyzing and improving the image quality of stylegan. In *Proceedings of the IEEE/CVF Conference on Computer Vision and Pattern Recognition*, pages 8110–8119, 2020.
- [4] Tero Karras, Samuli Laine, and Timo Aila. A style-based generator architecture for generative adversarial networks. In *Proceedings of the IEEE/CVF conference on computer vision and pattern recognition*, pages 4401–4410, 2019.
- [5] Yunjey Choi, Youngjung Uh, Jaejun Yoo, and Jung-Woo Ha. Stargan v2: Diverse image synthesis for multiple domains. In *Proceedings of the IEEE Conference on Computer Vision and Pattern Recognition*, 2020.
- [6] Jun-Yan Zhu, Taesung Park, Phillip Isola, and Alexei A Efros. Unpaired image-to-image translation using cycle-consistent adversarial networks. In *Proceedings of the IEEE international conference on computer vision*, pages 2223–2232, 2017.
- [7] Ming-Yu Liu, Xun Huang, Arun Mallya, Tero Karras, Timo Aila, Jaakko Lehtinen, and Jan Kautz. Few-shot unsupervised image-to-image translation. In *Proceedings of the IEEE/CVF International Conference on Computer Vision*, pages 10551–10560, 2019.
- [8] Ji Lin, Richard Zhang, Frieder Ganz, Song Han, and Jun-Yan Zhu. Anycost gans for interactive image synthesis and editing. In *Proceedings of the IEEE/CVF Conference on Computer Vision and Pattern Recognition*, pages 14986–14996, 2021.
- [9] Hongyu Liu, Ziyu Wan, Wei Huang, Yibing Song, Xintong Han, Jing Liao, Bin Jiang, and Wei Liu. Deflocnet: Deep image editing via flexible low-level controls. In *Proceedings of the IEEE/CVF Conference on Computer Vision and Pattern Recognition*, pages 10765–10774, 2021.
- [10] Swee Kiat Lim, Yi Loo, Ngoc Trung Tran, Ngai Man Cheung, Gemma Roig, and Yuval Elovici. Doping: Generative data augmentation for unsupervised anomaly detection with gan. In *18th IEEE International Conference on Data Mining, ICDM 2018*, pages 1122–1127. Institute of Electrical and Electronics Engineers Inc., 2018.
- [11] Ngoc-Trung Tran, Viet-Hung Tran, Ngoc-Bao Nguyen, Trung-Kien Nguyen, and Ngai-Man Cheung. On data augmentation for gan training. *IEEE Transactions on Image Processing*, 30:1882–1897, 2021.
- [12] Lucy Chai, Jun-Yan Zhu, Eli Shechtman, Phillip Isola, and Richard Zhang. Ensembling with deep generative views. In *CVPR*, 2021.
- [13] Qianli Feng, Chenqi Guo, Fabian Benitez-Quiroz, and Aleix M Martinez. When do gans replicate? on the choice of dataset size. In *Proceedings of the IEEE/CVF International Conference on Computer Vision*, pages 6701–6710, 2021.
- [14] Utkarsh Ojha, Yijun Li, Jingwan Lu, Alexei A Efros, Yong Jae Lee, Eli Shechtman, and Richard Zhang. Few-shot image generation via cross-domain correspondence. In *Proceedings of the IEEE/CVF Conference on Computer Vision and Pattern Recognition*, pages 10743–10752, 2021.
- [15] Atsuhiko Noguchi and Tatsuya Harada. Image generation from small datasets via batch statistics adaptation. In *Proceedings of the IEEE/CVF International Conference on Computer Vision*, pages 2750–2758, 2019.
- [16] Yaxing Wang, Chenshen Wu, Luis Herranz, Joost van de Weijer, Abel Gonzalez-Garcia, and Bogdan Raducanu. Transferring gans: generating images from limited data. In *Proceedings of the European Conference on Computer Vision (ECCV)*, pages 218–234, 2018.
- [17] Sangwoo Mo, Minsu Cho, and Jinwoo Shin. Freeze the discriminator: a simple baseline for fine-tuning gans. In *CVPR AI for Content Creation Workshop*, 2020.
- [18] Yijun Li, Richard Zhang, Jingwan (Cynthia) Lu, and Eli Shechtman. Few-shot image generation with elastic weight consolidation. In H. Larochelle, M. Ranzato, R. Hadsell, M. F. Balcan, and H. Lin, editors, *Advances in Neural Information Processing Systems*, volume 33, pages 15885–15896. Curran Associates, Inc., 2020.

- [19] Yunqing Zhao, Henghui Ding, Houjing Huang, and Ngai-Man Cheung. A closer look at few-shot image generation. In *CVPR*, 2022.
- [20] Sinno Jialin Pan and Qiang Yang. A survey on transfer learning. *IEEE Transactions on knowledge and data engineering*, 22(10):1345–1359, 2009.
- [21] Jia Deng, Wei Dong, Richard Socher, Li-Jia Li, Kai Li, and Li Fei-Fei. Imagenet: A large-scale hierarchical image database. In *2009 IEEE conference on computer vision and pattern recognition*, pages 248–255, 2009.
- [22] Jordan Yaniv, Yael Newman, and Ariel Shamir. The face of art: landmark detection and geometric style in portraits. *ACM Transactions on graphics (TOG)*, 38(4):1–15, 2019.
- [23] Alexander Ly, Maarten Marsman, Josine Verhagen, Raoul PPP Grasman, and Eric-Jan Wagenmakers. A tutorial on fisher information. *Journal of Mathematical Psychology*, 80:40–55, 2017.
- [24] Chelsea Finn, Pieter Abbeel, and Sergey Levine. Model-agnostic meta-learning for fast adaptation of deep networks. In *International conference on machine learning*, pages 1126–1135. PMLR, 2017.
- [25] Li Fei-Fei, Rob Fergus, and Pietro Perona. One-shot learning of object categories. *IEEE transactions on pattern analysis and machine intelligence*, 28(4):594–611, 2006.
- [26] Jake Snell, Kevin Swersky, and Richard Zemel. Prototypical networks for few-shot learning. In *Advances in neural information processing systems*, pages 4077–4087, 2017.
- [27] Yiluan Guo and Ngai-Man Cheung. Attentive weights generation for few shot learning via information maximization. In *Proceedings of the IEEE/CVF Conference on Computer Vision and Pattern Recognition*, pages 13499–13508, 2020.
- [28] Jiamei Sun, Sebastian Lapuschkin, Wojciech Samek, Yunqing Zhao, Ngai-Man Cheung, and Alexander Binder. Explanation-guided training for cross-domain few-shot classification. In *2020 25th International Conference on Pattern Recognition (ICPR)*, pages 7609–7616. IEEE, 2021.
- [29] Milad Abdollahzadeh, Touba Malekzadeh, and Ngai-Man Man Cheung. Revisit multimodal meta-learning through the lens of multi-task learning. *Advances in Neural Information Processing Systems*, 35, 2021.
- [30] Yunqing Zhao and Ngai-Man Cheung. Fs-ban: Born-again networks for domain generalization few-shot classification. *arXiv preprint arXiv:2208.10930*, 2022.
- [31] Weide Liu, Chi Zhang, Guosheng Lin, and Fayao Liu. Crnet: Cross-reference networks for few-shot segmentation. In *Proceedings of the IEEE/CVF Conference on Computer Vision and Pattern Recognition*, pages 4165–4173, 2020.
- [32] Malik Boudiaf, Hoel Kervadec, Ziko Imtiaz Masud, Pablo Piantanida, Ismail Ben Ayed, and Jose Dolz. Few-shot segmentation without meta-learning: A good transductive inference is all you need? In *Proceedings of the IEEE/CVF Conference on Computer Vision and Pattern Recognition*, pages 13979–13988, 2021.
- [33] Gongjie Zhang, Kaiwen Cui, Rongliang Wu, Shijian Lu, and Yonghong Tian. Pnpdet: Efficient few-shot detection without forgetting via plug-and-play sub-networks. In *Proceedings of the IEEE/CVF Winter Conference on Applications of Computer Vision*, pages 3823–3832, 2021.
- [34] Zhibo Fan, Yuchen Ma, Zeming Li, and Jian Sun. Generalized few-shot object detection without forgetting. In *Proceedings of the IEEE/CVF Conference on Computer Vision and Pattern Recognition*, pages 4527–4536, 2021.
- [35] Jia Gong, Zhipeng Fan, Qihong Ke, Hossein Rahmani, and Jun Liu. Meta agent teaming active learning for pose estimation. In *Proceedings of the IEEE/CVF Conference on Computer Vision and Pattern Recognition*, pages 11079–11089, 2022.
- [36] Tero Karras, Miika Aittala, Janne Hellsten, Samuli Laine, Jaakko Lehtinen, and Timo Aila. Training generative adversarial networks with limited data. *Advances in Neural Information Processing Systems*, 33:12104–12114, 2020.
- [37] Christian Szegedy, Vincent Vanhoucke, Sergey Ioffe, Jon Shlens, and Zbigniew Wojna. Rethinking the inception architecture for computer vision. In *Proceedings of the IEEE conference on computer vision and pattern recognition*, pages 2818–2826, 2016.
- [38] Richard Zhang, Phillip Isola, Alexei A Efros, Eli Shechtman, and Oliver Wang. The unreasonable effectiveness of deep features as a perceptual metric. In *CVPR*, 2018.

- [39] Alex Krizhevsky, Ilya Sutskever, and Geoffrey E Hinton. Imagenet classification with deep convolutional neural networks. *Advances in neural information processing systems*, 25:1097–1105, 2012.
- [40] Laurens van der Maaten and Geoffrey Hinton. Visualizing data using t-sne. *Journal of Machine Learning Research*, 9(86):2579–2605, 2008.
- [41] Hossein Talebi and Peyman Milanfar. Learned perceptual image enhancement. In *2018 IEEE international conference on computational photography (ICCP)*, pages 1–13. IEEE, 2018.
- [42] Hossein Talebi and Peyman Milanfar. Nima: Neural image assessment. *IEEE transactions on image processing*, 27(8):3998–4011, 2018.
- [43] Stanislav Morozov, Andrey Voynov, and Artem Babenko. On self-supervised image representations for {gan} evaluation. In *International Conference on Learning Representations*, 2021.
- [44] Martin Heusel, Hubert Ramsauer, Thomas Unterthiner, Bernhard Nessler, and Sepp Hochreiter. Gans trained by a two time-scale update rule converge to a local nash equilibrium. *Advances in neural information processing systems*, 30, 2017.
- [45] David Bau, Jun-Yan Zhu, Hendrik Strobelt, Bolei Zhou, Joshua B Tenenbaum, William T Freeman, and Antonio Torralba. Gan dissection: Visualizing and understanding generative adversarial networks. In *Proceedings of the International Conference on Learning Representations (ICLR)*, 2019.
- [46] David Bau, Bolei Zhou, Aditya Khosla, Aude Oliva, and Antonio Torralba. Network dissection: Quantifying interpretability of deep visual representations. In *Proceedings of the IEEE conference on computer vision and pattern recognition*, pages 6541–6549, 2017.
- [47] Alessandro Achille, Michael Lam, Rahul Tewari, Avinash Ravichandran, Subhansu Maji, Charless C Fowlkes, Stefano Soatto, and Pietro Perona. Task2vec: Task embedding for meta-learning. In *Proceedings of the IEEE/CVF International Conference on Computer Vision*, pages 6430–6439, 2019.
- [48] Christian Simon, Piotr Koniusz, Richard Nock, and Mehrtash Harandi. On modulating the gradient for meta-learning. In *European Conference on Computer Vision*, pages 556–572. Springer, 2020.
- [49] Keshigeyan Chandrasegaran, Ngoc-Trung Tran, Alexander Binder, and Ngai-Man Cheung. Discovering Transferable Forensic Features for CNN-generated Images Detection. In *Proceedings of the European Conference on Computer Vision (ECCV)*, Oct 2022.
- [50] Sheng-Yu Wang, Oliver Wang, Richard Zhang, Andrew Owens, and Alexei A. Efros. CNN-Generated Images Are Surprisingly Easy to Spot... for Now. In *IEEE/CVF Conference on Computer Vision and Pattern Recognition (CVPR)*, June 2020.
- [51] Keshigeyan Chandrasegaran, Ngoc-Trung Tran, and Ngai-Man Cheung. A Closer Look at Fourier Spectrum Discrepancies for CNN-Generated Images Detection. In *Proceedings of the IEEE/CVF Conference on Computer Vision and Pattern Recognition (CVPR)*, pages 7200–7209, June 2021.
- [52] Joel Frank, Thorsten Eisenhofer, Lea Schönherr, Asja Fischer, Dorothea Kolossa, and Thorsten Holz. Leveraging frequency analysis for deep fake image recognition. In *International conference on machine learning*, pages 3247–3258. PMLR, 2020.
- [53] Geoffrey Hinton, Oriol Vinyals, and Jeffrey Dean. Distilling the knowledge in a neural network. In *NIPS Deep Learning and Representation Learning Workshop*, 2015.
- [54] Keshigeyan Chandrasegaran, Ngoc-Trung Tran, Yunqing Zhao, and Ngai-Man Cheung. Revisiting Label Smoothing and Knowledge Distillation Compatibility: What was Missing? In Kamalika Chaudhuri, Stefanie Jegelka, Le Song, Csaba Szepesvari, Gang Niu, and Sivan Sabato, editors, *Proceedings of the 39th International Conference on Machine Learning*, volume 162 of *Proceedings of Machine Learning Research*, pages 2890–2916. PMLR, 17-23 Jul 2022.
- [55] Byeongho Heo, Jeessoo Kim, Sangdoo Yun, Hyojin Park, Nojun Kwak, and Jin Young Choi. A comprehensive overhaul of feature distillation. In *Proceedings of the IEEE/CVF International Conference on Computer Vision*, pages 1921–1930, 2019.
- [56] Utku Evci, Vincent Dumoulin, Hugo Larochelle, and Michael C Mozer. Head2toe: Utilizing intermediate representations for better transfer learning. In *International Conference on Machine Learning*, pages 6009–6033. PMLR, 2022.
- [57] Ngoc-Trung Tran, Tuan-Anh Bui, and Ngai-Man Cheung. Dist-gan: An improved gan using distance constraints. In *Proceedings of the European Conference on Computer Vision (ECCV)*, pages 370–385, 2018.

- [58] Hung-Yu Tseng, Lu Jiang, Ce Liu, Ming-Hsuan Yang, and Weilong Yang. Regularizing generative adversarial networks under limited data. In *Proceedings of the IEEE/CVF Conference on Computer Vision and Pattern Recognition*, pages 7921–7931, 2021.
- [59] Miaoyun Zhao, Yulai Cong, and Lawrence Carin. On leveraging pretrained gans for generation with limited data. In *International Conference on Machine Learning*, pages 11340–11351. PMLR, 2020.
- [60] Yulai Cong, Miaoyun Zhao, Jianqiao Li, Sijia Wang, and Lawrence Carin. Gan memory with no forgetting. *Advances in Neural Information Processing Systems*, 33:16481–16494, 2020.
- [61] Maria-Elena Nilsback and Andrew Zisserman. Automated flower classification over a large number of classes. In *2008 Sixth Indian Conference on Computer Vision, Graphics & Image Processing*, pages 722–729. IEEE, 2008.
- [62] X. Huang and S. Belongie. Arbitrary style transfer in real-time with adaptive instance normalization. In *ICCV*, 2017.
- [63] Oriol Vinyals, Charles Blundell, Timothy Lillicrap, Daan Wierstra, et al. Matching networks for one shot learning. In *NeurIPS*, pages 3630–3638, 2016.
- [64] Tero Karras, Timo Aila, Samuli Laine, and Jaakko Lehtinen. Progressive growing of gans for improved quality, stability, and variation. *arXiv preprint arXiv:1710.10196*, 2017.
- [65] Karen Simonyan, Andrea Vedaldi, and Andrew Zisserman. Deep inside convolutional networks: Visualising image classification models and saliency maps. *arXiv preprint arXiv:1312.6034*, 2013.
- [66] Haoliang Li, Sinno Jialin Pan, Shiqi Wang, and Alex C Kot. Domain generalization with adversarial feature learning. In *Proceedings of the IEEE Conference on Computer Vision and Pattern Recognition*, pages 5400–5409, 2018.
- [67] Fisher Yu, Yinda Zhang, Shuran Song, Ari Seff, and Jianxiong Xiao. Lsun: Construction of a large-scale image dataset using deep learning with humans in the loop. *arXiv preprint arXiv:1506.03365*, 2015.
- [68] Shengyu Zhao, Zhijian Liu, Ji Lin, Jun-Yan Zhu, and Song Han. Differentiable augmentation for data-efficient gan training. *Advances in Neural Information Processing Systems*, 33:7559–7570, 2020.

Acknowledgment

This project is partially supported by the grant RS-INSUR-00027. This work was also supported in part by the National Research Foundation, Singapore, under its AI Singapore Programmes (AISG) under Award AISG2-RP-2021-021 and Award AISG-100E2018-005; and in part by the Singapore University of Technology and Design under Project PIE-SGP-AI-2018-01. We thank anonymous reviewers for their insightful comments.

Supplementary Material

This Supplementary provides additional experiments, results, analysis and ablation studies to further support our contributions. The Supplementary materials are organized as follows:

- Section 7: Proposed Importance Probing Algorithm : Details
 - Section 7.1 Computational Overhead
 - Section 7.2 Illustration of Kernel Modulation Operations
 - Section 7.3 Fisher Information approximation using proxy vectors
- Section 8: Discussion on Related Works
- Section 9: Ablation Studies and Additional Analysis on Importance Probing
- Section 10: Extended Experiments and Results (and Visualizations)
 - Section 10.1: Additional Source / Target Domain Setups
 - Section 10.2: Additional GAN Architectures
 - Section 10.3: Alternative characterization of importance measure
 - Section 10.4: Comparison with Adaptive Data Augmentation
 - Section 10.5: Importance probing with extremely limited number of samples
- Section 11: Discussion: What form of visual information is encoded by high FI kernels?
- Section 12: Main Paper Experiments : Additional Results / Analysis
 - Section 12.1: KID / Intra-LPIPS / Standard Deviation of Experiments
 - Section 12.2: 10-shot Adaptation Results
 - Section 12.4: FID measurements with limited target domain samples
- Section 13: Discussion: How much the proximity between the source and the target could be relaxed?
- Section 14: Additional information for Checklist
 - Section 14.1: Potential Societal Impact
 - Section 14.2: Amount of Compute

Reproducibility. Project Page: <https://yunqing-me.github.io/AdAM/>.

Table 3: Comparison of training cost in terms of number of trainable parameters, training iterations and compute time for different FSIG methods. FFHQ is the source domain and we show results for Babies (top) and Cat (bottom) target domains. One can clearly observe that our proposed IP is extremely lightweight and our KML based adaptation contains much less trainable parameters in the source GAN. All results are measured in containerized environments using a single Tesla V100-PCIE (32 GB) GPU with batch size of 4. All reported results are averaged over 3 independent runs.

FFHQ \rightarrow Babies				
Method	Stage	# trainable params (M)	# iteration	# time
TGAN [16]	Adaptation	30.0	3000	110 mins
FreezeD [17]	Adaptation	30.0	3000	110 mins
EWC [18]	Adaptation	30.0	3000	110 mins
CDC [14]	Adaptation	30.0	3000	120 mins
DCL [19]	Adaptation	30.0	3000	120 mins
AdAM (Ours)	IP	0.105	500	8 mins
	Adaptation	18.9	1500	65min

FFHQ \rightarrow AFHQ-Cat				
Method	Stage	# trainable params (M)	# iteration	# time
TGAN [16]	Adaptation	30.0	6000	210 mins
FreezeD [17]	Adaptation	30.0	6000	200 mins
EWC [18]	Adaptation	30.0	6000	220 mins
CDC [14]	Adaptation	30.0	6000	300 mins
DCL [19]	Adaptation	30.0	6000	300 mins
AdAM (Ours)	IP	0.105	500	8 mins
	Adaptation	18.9	2500	110 mins

7 Proposed Importance Probing Algorithm: Details

7.1 Computational Overhead

Our proposed Importance Probing (IP) algorithm to measure the importance of each individual kernel in the source GAN for the target-domain is lightweight. *i.e.*: proposed importance probing only requires 8 minutes compared to the adaptation step which requires \approx 110 minutes (Averaged over 3 runs for FFHQ \rightarrow Cat adaptation experiment). This is achieved using two design choices:

- During IP, only modulation parameters are updated. Given that our modulation design is low-rank KML, the number of trainable parameters is significantly small compared to the actual source GAN. *i.e.*: number of trainable parameters in our proposed IP is only 0.1M whereas the source GAN contains 30.0M trainable parameters.
- Our proposed IP is performed for limited number of iterations to measure the importance for the target domain. *i.e.*: IP stage requires only 500 iterations to achieve a good performance for adaptation.

Complete details on number of trainable parameters and compute time for our proposed method and existing FSIG works are provided in Table 3. As one can observe, our proposed method (both IP and adaptation) is better than existing FSIG works in terms of trainable parameters and compute time.

7.2 Kernel Modulation (KML) with rank-constrained operations

Here we show more details of KML, as supplement to the main paper, as Figure 6.

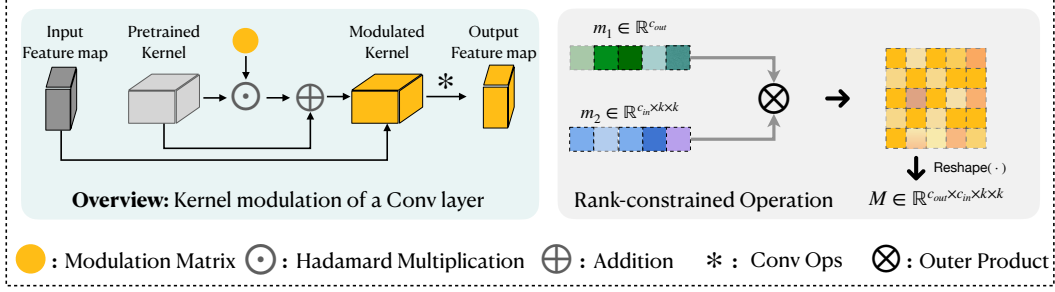


Figure 6: Illustration of Kernel Modulation operations. Here we use a convolutional kernel for instance. Similar operations are applied to the linear layer.

7.3 Fisher Information Approximation Using Proxy Vectors

Recall in Sec.4 of main paper, we consider low-rank approximation of modulation matrix using outer product of proxy vectors: $\mathbf{M}_i = \text{reshape}([\mathbf{m}_1^i \mathbf{m}_2^1, \dots, \mathbf{m}_1^i \mathbf{m}_2^{c_{in} \times k \times k}])$, where $|\mathbf{m}_2| = (c_{in} \times k \times k)$. In order to calculate the FI of the modulation matrix, we start with the FI of each element in this matrix. Considering $m_{ij} = \mathbf{m}_1^i \mathbf{m}_2^j$, following equation can be derived by simple application of chain rule of differentiation:

$$\frac{\partial \mathcal{L}}{\partial m_{ij}} = \frac{1}{2\mathbf{m}_2^j} \frac{\partial \mathcal{L}}{\partial \mathbf{m}_1^i} + \frac{1}{2\mathbf{m}_1^i} \frac{\partial \mathcal{L}}{\partial \mathbf{m}_2^j} \quad (4)$$

We use the square of the gradients to estimate the FI [47]. Therefore, the following equation can be obtained between the FI of these variables:

$$\mathcal{F}(m_{ij}) = \frac{1}{4\mathbf{m}_2^{j^2}} \mathcal{F}(\mathbf{m}_1^i) + \frac{1}{4\mathbf{m}_1^{i^2}} \mathcal{F}(\mathbf{m}_2^j) + \frac{1}{2\mathbf{m}_1^i \mathbf{m}_2^j} \frac{\partial \mathcal{L}}{\partial \mathbf{m}_1^i} \frac{\partial \mathcal{L}}{\partial \mathbf{m}_2^j} \quad (5)$$

Then, the FI of the modulation matrix $\mathbf{M}_i = [m_{i1}, m_{i2}, \dots]$, can be calculated as:

$$\begin{aligned} \mathcal{F}(\mathbf{M}_i) &= \sum_{j=1}^{|\mathbf{m}_2|} \mathcal{F}(m_{ij}) \\ &= \sum_{j=1}^{|\mathbf{m}_2|} \left(\frac{1}{4\mathbf{m}_2^{j^2}} \mathcal{F}(\mathbf{m}_1^i) + \frac{1}{4\mathbf{m}_1^{i^2}} \mathcal{F}(\mathbf{m}_2^j) + \frac{1}{2\mathbf{m}_1^i \mathbf{m}_2^j} \frac{\partial \mathcal{L}}{\partial \mathbf{m}_1^i} \frac{\partial \mathcal{L}}{\partial \mathbf{m}_2^j} \right) \\ &= \mathcal{F}(\mathbf{m}_1^i) \sum_{j=1}^{|\mathbf{m}_2|} \frac{1}{4\mathbf{m}_2^{j^2}} + \frac{1}{4\mathbf{m}_1^{i^2}} \sum_{j=1}^{|\mathbf{m}_2|} \mathcal{F}(\mathbf{m}_2^j) \\ &\quad + \frac{1}{2\mathbf{m}_1^i} \frac{\partial \mathcal{L}}{\partial \mathbf{m}_1^i} \sum_{j=1}^{|\mathbf{m}_2|} \frac{1}{\mathbf{m}_2^j} \frac{\partial \mathcal{L}}{\partial \mathbf{m}_2^j} \end{aligned} \quad (6)$$

We empirically observed that discarding (i) the cross-term (ii) the coefficients $(\frac{1}{4\mathbf{m}_2^{j^2}}, \frac{1}{4\mathbf{m}_1^{i^2}})$ in the importance of each kernel in Eqn. 6 results in a similar FID for the final adapted model. Therefore, the estimation can be simpler and more lightweight. In particular, the following (simpler) estimated version of $\mathcal{F}(\mathbf{M}_i)$ is used in our work:

$$\hat{\mathcal{F}}(\mathbf{M}_i) = \mathcal{F}(\mathbf{m}_1^i) + \frac{1}{|\mathbf{m}_2|} \sum_{j=1}^{|\mathbf{m}_2|} \mathcal{F}(\mathbf{m}_2^j) \quad (7)$$

Note that $\hat{\mathcal{F}}(\mathbf{M}_i)$ intuitively estimates the FI of the modulation matrix by a weighted average of its constructing parameters corresponding to their occurrence frequency in calculation of \mathbf{M}_i . We remark that in our implementation, for reporting all of the results in the main paper, and also the additional results in the supplementary, we have used this lightweight estimation Eqn. 7 to calculate the importance of each kernel during importance probing.

8 Discussion of Related Works

In Sec.2 of the main paper, we discuss closely-related work of this paper that focuses on few-shot image generation (FSIG) under extremely limited data, i.e., 10 samples. Here, we review other related work.

8.1 Image generation with less data

Since the introduction of GANs [1], there is a fair amount of work to focus on training of GANs with less data in recent literature, with efforts on introducing additional data augmentation methods [36, 57], regularization terms [58], modifying GAN architectures [59], and modification of filter kernels [59, 60]. Commonly, these works focus on setups with several thousands of images, i.e.: Flowers dataset [61] with 8,189 images in [60], 10% of ImageNet, or the entire AFHQ [5] dataset. On the other hand, FSIG with extremely limited data (10 samples) poses unique challenges. In particular, as pointed out in [14, 19], severe mode collapse and loss in diversity are critical challenges in FSIG that require special attention. We remark that in [60], a technique called AdaFM is introduced to update kernels. However, the underlying ideas and mechanism of AdaFM and our KML are quite different. AdaFM is inspired from style-transfer literature [62], introduces independent scale and shift (scalar) parameters to update individual channels of kernels to manipulate their styles. On the other hand, as discussed in the main paper, KML introduces a structural $\mathbf{J} + \mathbf{M}$, $\mathbf{M} = \mathbf{m}_1 \otimes \mathbf{m}_2$, to update multiple kernels in a coordinated manner. In our experiment, we also test AdaFM in few-shot setups and compare its performance with KML.

8.2 Discriminative kernel modulation

As mentioned in the main paper, Kernel Modulation (KML) is originally proposed in [29] for adapting the model between different modes of few-shot classification (FSC) tasks. However, due to some differences between the multimodal meta-learner in [29], and our transfer learning-based scheme, there are important differences in design choices when applying KML to our problem. **First**, in contrast to FSC work [29] which follows a *discriminative learning* setup, we aim to address a problem in a *generative learning* setup. **Second**, in FSC setup, the modulation parameters are generated during adaptation to target task with a pretrained modulation network trained on tens of thousands of few-shot tasks. So the modulation parameters are not directly learned for a target few-shot task. In contrast, in our setup, the base kernel is frozen during the adaptation, and we directly learn the modulation parameters for a target domain/task using a very limited number of samples (e.g., 10-shot). **Finally**, in FSC, usually source and target tasks follow a same task distribution $p(\mathcal{T})$. In fact, in implementation, even though the classes are disjoint between source and target tasks, all of them are constructed using the data from the same domain (e.g., miniImageNet [63]). However, in our setup, the source and target tasks/domains distributions could be very different (e.g., Human Faces (FFHQ) \rightarrow Cats).

9 Ablation Studies and Additional Analysis on Importance Probing

In this section, we conduct extensive ablation studies to show the significance of our proposed method for FSIG. Similar to main paper analysis, we use FFHQ [3] as the source domain, and use Babies and Cat [5] as target domains. The different approaches in the study are as follows:

- TGAN [16]: The source GAN models pretrained on FFHQ are updated using *simple fine-tuning* with the 10 shot target samples.
- EWC [18]: Following [18], a L2 regularization is applied to all model weights to augment simple fine-tuning. The regularization is scaled by the importance of individual model weights as determined by the FI of the model weights based on the *source* models.

- EWC + IP: We apply our probing idea on top of EWC. In the probing step, original EWC as discussed above is used but with a small number of iterations. At the end of probing, FI of the model weights based on the *updated* models is computed. Then, during main adaptation, this *target-aware* FI is used to scale the L2 regularization. In other words, EWC + IP is a target-aware version of EWC in [18] using our probing idea.
- AdaFM [60]: AdaFM modulation is applied to all kernels.
- AdaFM + IP: We apply our probing idea on top of AdaFM. In the probing step, original AdaFM as discussed above is used but with a small number of iterations. At the end of probing, FI of AdaFM parameters is computed, and kernels are classified as important/unimportant using the same 75% quantile threshold as in our work. Then, during main adaptation, the important kernels are updated via AdaFM, and the unimportant kernels are updated via simple fine tuning. In other words, AdaFM + IP is a target-aware version of AdaFM using our probing idea.
- Ours w/o IP (*i.e.* main adaptation only): KML modulation is applied to all kernels.
- Ours w/ Freeze: We apply our probing idea as discussed in the main paper, *i.e.*, with KML applied to all kernels but adaptation with a small number of iterations. At the end of probing, FI of KML parameters is computed, and kernels are classified as important/unimportant using the same 75% quantile threshold as in our work. Then, during main adaptation, the important kernels are *frozen*, and the unimportant kernels are updated via simple fine tuning. In other words, this is similar to our proposed method except that kernel freezing is used in main adaptation instead of KML for important kernels.
- Ours w/ KML (*i.e.* our main proposed method): This is the method proposed in the main paper. We apply our probing idea as discussed in the main paper, *i.e.*, with KML applied to all kernels but adaptation with a small number of iterations. At the end of probing, FI of KML parameters is computed, and kernels are classified as important/unimportant using 75% quantile threshold. Then, during main adaptation, the important kernels are modulated using KML, and the unimportant kernels are updated via simple fine tuning.

Qualitative Results. We show generated images corresponding to all approaches discussed above in Figure 7. These results show that our proposed idea on importance probing is principally a suitable approach to improve FSIG by identifying kernels important for target domain adaptation. Figure 7 also shows that our proposed method can generate images with better quality.

Quantitative results. We show FID / LPIPS results in Table 4. These results show that our proposed IP is principally a suitable approach for FSIG. This can be clearly observed when applying IP to EWC [18] and AdaFM [60]. We remark that probing with KML (ours AdAM) is computationally much efficient compared to probing with EWC and AdaFM due to less number of trainable parameters. Overall, we quantitatively show that our proposed method outperforms existing FSIG methods with IP, thereby generating images with a good balance between quality (FID ↓) and diversity (Intra-LPIPS ↑). We also empirically observe that methods performing IP at kernel level (Ours w/ KML, AdaFM + IP) perform better than method performing IP at parameter level (EWC + IP).

10 Extended Experiments and Results

In this section, we conduct additional experiments to further support our findings and contributions.

10.1 Additional source / target domains

Following [14], we conduct extended experiments using Church as the source domain. [14] uses Haunted houses and Van Gogh Houses as target domains. Similar to Sec.3 in the main paper, our analysis confirms that these target domains are closer to the source domain (Church). We additionally include palace and yurt as target domains to relax the close proximity assumption. Proximity visualization is shown in Figure 8.

Experiment Details. For fair comparison, we strictly follow prior works [16–18, 14, 19] in the choice of GAN architecture, source-target adaptation setups and hyper-parameters. We use StyleGAN-V2 [3] as the GAN architecture and FFHQ as the source domain. We use 256 x 256 resolution for adaptation. Adaptation is performed with batch size 4 on a single Tesla V100 GPU. We apply importance probing

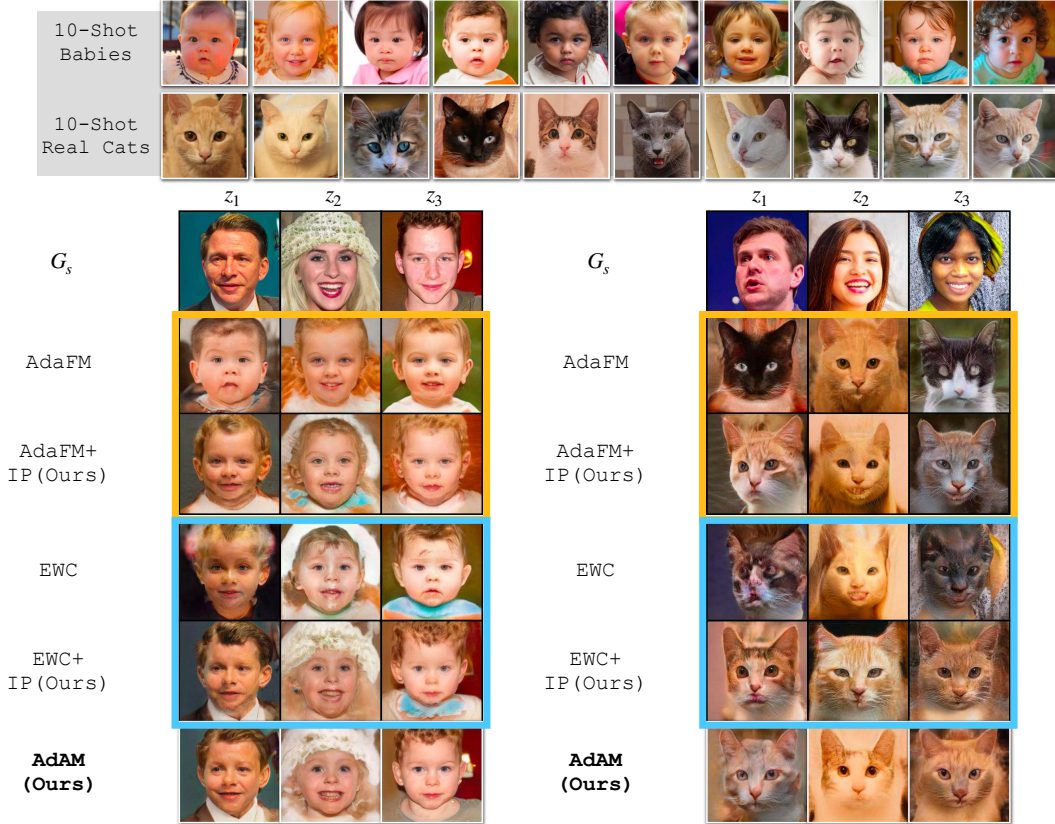


Figure 7: G_s is the source generator (FFHQ). We show results for FFHQ \rightarrow Babies (left) and FFHQ \rightarrow Cat (right), similar to the main paper. Applying our idea of importance probing to EWC [18], AdaFM [60], we observe better quality in FSIG. This shows that our proposed idea on importance probing is principally a suitable approach to improve FSIG. One can also observe that images generated by our proposed method (with KML) has good quality compared to other methods. This is quantitatively confirmed in Table 4.

and modulation on base kernels of both generator and discriminator. We focus on 10-shot target adaptation setup.

Results. Given that the target domain only contains 10 real images, following [14], we show the quality of FSIG for 10-shot adaption. Qualitative analysis is shown in Figure 24. As one can observe, SOTA FSIG methods [18, 14, 19] are unable to adapt well to distant target domain (palace) due to *due to only considering source domain / task in knowledge preservation*. We remark that TGAN [16] suffers severe mode collapse. We clearly show that our proposed adaptation-aware FSIG method outperforms existing FSIG works.

Further, we show complete 10-shot adaptation results. Results for Haunted Houses, Van Gogh Houses, Palace and Yurt are shown in Figures 9, 10, 12, 11 respectively. Other adaptation setups with FFHQ/Cars as source are shown in Figure 25, Figure 26, Figure 27, Figure 28, Figure 29, Figure 30 and Figure 31.

10.2 Additional GAN Architectures

We use an additional pre-trained GAN architecture, ProGAN [64], to conduct FSIG experiments for FFHQ \rightarrow Babies, FFHQ \rightarrow Cat, Church \rightarrow Haunted houses and Church \rightarrow Palace setups. For fair comparison, we strictly follow the exact experiment setup discussed in Section 10.1.

Results. We show complete qualitative and quantitative results for FFHQ \rightarrow Babies, FFHQ \rightarrow Cat adaptation in Figures 13 and 14 respectively. As one can observe, our proposed method consistently outperforms other baseline and SOTA FSIG methods with another pre-trained GAN model (ProGAN

Table 4: Ablation studies for IP: FFHQ [3] is the source domain. We use Babies and Cats [5] as target domains. We show FID (left) and Intra-LPIPS (right) results. For each method, best FID and LPIPS results are shown in **bold**. IP is performed for 500 iterations (where relevant). These results show that our proposed IP is principally a suitable approach for FSIG. This can be clearly observed when applying IP to EWC [18] (EWC+IP) and AdaFM [60] (AdaFM+IP). We also observe that methods performing IP at kernel level (Ours w/ KML, AdaFM + IP) perform better than method performing IP at parameter level (EWC + IP). Overall, we quantitatively show that our proposed method outperforms all existing FSIG methods with IP, thereby generating images with high quality (FID) and diversity (Intra-LPIPS).

Target Domain	Babies FID (↓)	Cat FID (↓)	Target Domain	Babies Intra-LPIPS (↑)	Cat Intra-LPIPS (↑)
TGAN [16]	101.58	64.68	TGAN [16]	0.517	0.490
EWC [18]	79.93	74.61	EWC [18]	0.521	0.587
EWC + [IP (Ours)]	70.80	66.35	EWC + [IP (Ours)]	0.625	0.540
AdaFM [60]	62.90	64.44	AdaFM [60]	0.568	0.525
AdaFM + [IP (Ours)]	55.64	60.04	AdaFM + [IP (Ours)]	0.577	0.540
Ours w/o IP	54.46	82.41	Ours w/o IP	0.613	0.522
Ours w/ Freeze [w/ IP]	50.81	61.60	Ours w/ Freeze [w/ IP]	0.581	0.559
AdAM (w/ KML [w/ IP])	48.83	58.07	AdAM (w/ KML [w/ IP])	0.590	0.557

[64]), demonstrating the effectiveness and generalizability of our method. We also show qualitative results for Church → Haunted houses and Church → Palace adaptation in Figures 15 and 16 respectively.

10.3 Alternative characterization of importance measure

In literature, Class Saliency [65] (CS) is used as a property to explain which area/pixels of an input image stand out for a specific classification decision. Similar to the estimated Fisher Information (FI) used in our work, the complexity of CS is based on the first-order derivatives. Therefore, conceptually CS could have a connection with FI as they both use the knowledge encoded in the gradients.

We perform an experiment to replace FI with CS in importance probing and compare with our original approach. Note that, in [65], CS is computed w.r.t. input image pixels. To make CS suitable for our problem, we modify it and compute CS w.r.t. modulation parameters. Similar to our approach in the main paper, we average the importance of all parameters within a kernel to calculate the importance of that kernel. Then we use these values during our importance probing to determine the important kernels for adapting from source to target domain (as Sec. 4 in our main paper). The results in Table 5 are obtained with our proposed method using FI and CS during importance probing:

Table 5: In this experiment, we replace FI with CS in importance probing and compare with our original approach. We evaluate the performance under different source → target adaptation setups.

Domain	FFHQ → Babies		FFHQ → Cat	
	FID (↓)	Intra-LPIPS (↑)	FID (↓)	Intra-LPIPS (↑)
Class Saliency [65]	52.46	0.582	61.68	0.556
Fisher Information (Ours)	48.83	0.590	58.07	0.557

Our results suggest that importance probing using FI (approximated by first-order derivatives) can perform better in selection of important kernels, leading to better performance (FID, intra-LPIPS) in the adapted models as shown in the Table 5.

10.4 Comparison with Adaptive Data Augmentation [36]

We additionally include the results of Adaptive Data Augmentation [36] (ADA), as a supplement to Figure 4 in the main paper. We show that our proposed method consistently outperforms ADA in few-shot adaptation setups. The results are shown in Figures 17 and 18.

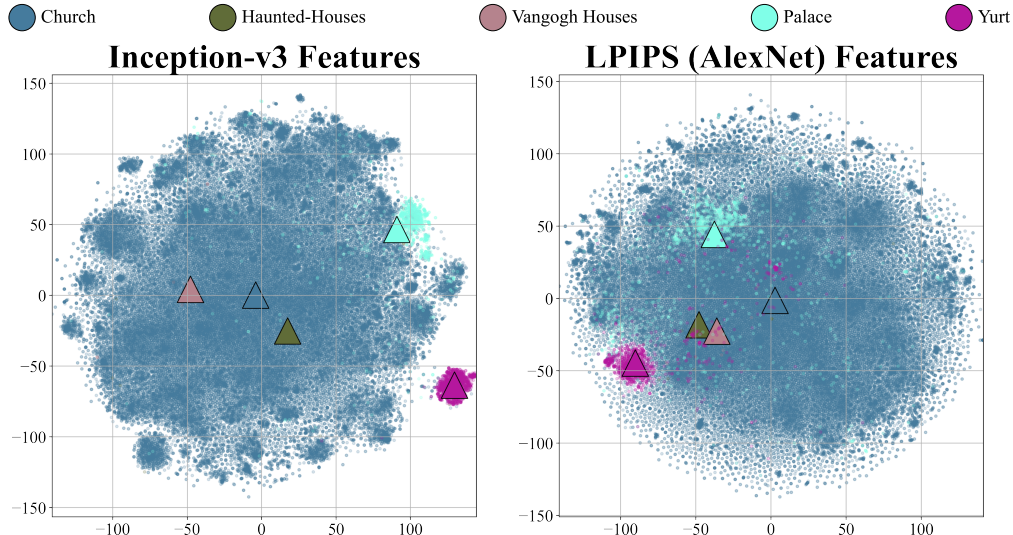


Figure 8: *Source-target domain proximity Visualization*: We use Church as the source domain following [14]. We show source-target domain proximity by visualizing Inception-v3 (Left) [37] and LPIPS (Middle) [38] –using AlexNet [39] backbone– features, and quantitatively using FID / LPIPS metrics (Right). For feature visualization, we use t-SNE [40] and show centroids (Δ) for all domains. FID / LPIPS is measured with respect to FFHQ. There are 2 important observations: ① Common target domains used in existing FSIG works (Haunted Houses, Van Gogh Houses) are notably proximal to the source domain (Church). This can be observed from the feature visualization and verified by FID / LPIPS measurements. ② We clearly show using feature visualizations and FID / LPIPS measurements that additional setups – Palace [21] and Yurt [21] – represent target domains that are distant from the source domain (Church). We remark that due to availability of only 10-shot samples in the target domain, FID / LPIPS are not measured in these setups.



Figure 9: Church \rightarrow Haunted House

10.5 Importance probing with extremely limited number of samples.

In Figure 6 (main paper), we perform ablation studies to show that our method consistently outperforms other baseline and SOTA methods given different number of target samples. In this section, we conduct additional experiments with extremely limited number of target samples: 1-shot and 5-shot. We also conduct experiments with more training samples during adaptation to show that our method consistently outperforms existing FSIG methods.

Results. The results are shown in Figure 19. Here we additionally include Adaptive Data Augmentation as an important baseline, and qualitative results can be found in Figures 17 and 18.



Figure 10: Church \rightarrow Van Gogh's House



Figure 11: Church \rightarrow Palace (distant domain)

11 Discussion: What form of visual information is encoded by high FI kernels?

In this section, we attempt to discover what form of visual information is encoded/generated by a specific high FI kernel identified by our importance probing method. This is a complex problem and to our best knowledge, methods on visualizing generative models/GANs are still rather restrictive in terms of concepts that can be visualized. Nevertheless, we leverage on GAN Dissection method [45], a more established visualization method to visualize the high FI internal representations.

Experiment setup: We use Church as the source domain as official GAN Dissection method ² is more suitable for scene-based image generation models (This is due to limitation of the semantic segmentation pipeline in GAN Dissection [45]). We use 2 target domains: haunted houses (proximal domain) and palace (distant domain). Following official GAN Dissection implementation [45], we use the ProGAN [64] model. For fair comparison, we strictly follow the exact experiment setup discussed in Section 10.1.

Results.

- Visualizing high FI kernels for Church \rightarrow Haunted Houses adaptation : The results for FI estimation for kernels and several distinct semantic concepts learnt by high FI kernels are shown in Figure 20. In Figure 20, we visualize four examples of high FI kernels: (a), (b), (c), (d) corresponding to concepts building, building, tree and wood respectively. Using GAN Dissection, we observe that a notable amount of high FI kernels correspond to useful source domain concepts including building, tree and wood (texture) which are preserved when adapting to Haunted Houses target domain. We remark that these preserved concepts are useful to the target domain for adaptation.
- Visualizing high FI kernels for Church \rightarrow Palace adaptation : The results for FI estimation for kernels and several distinct semantic concepts learnt by high FI kernels are shown in

²<https://github.com/CSAILVision/gandissect>



Figure 12: Church \rightarrow Yurt (distant domain)

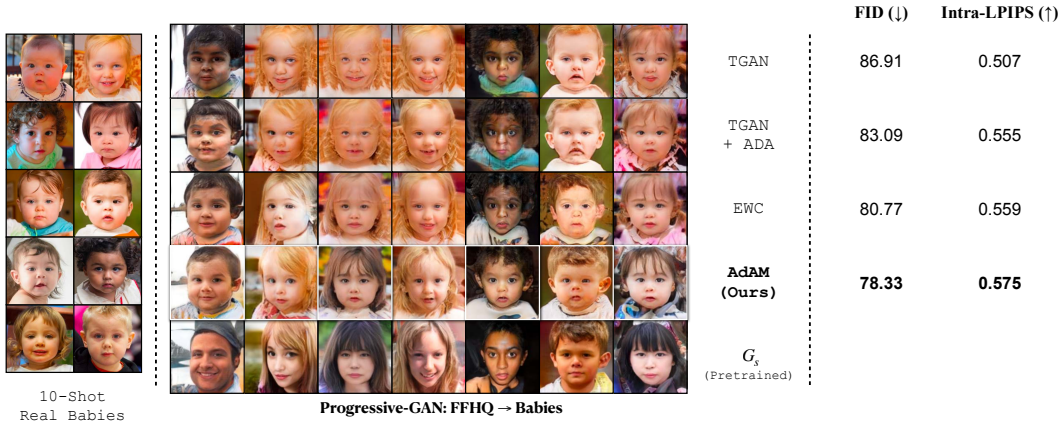


Figure 13: FFHQ \rightarrow Babies 10-shot adaptation results using pre-trained ProGAN [64] generator. We include ADA results. As one can observe, our proposed method outperforms existing FSIG methods.

Figure 21. In Figure 21, we visualize four examples of high FI kernels: (a), (b), (c), (d) corresponding to concepts grass, grass, building and building respectively. Using GAN Dissection, we observe that a notable amount of high FI kernels correspond to useful source domain concepts including grass and building which are preserved when adapting to Palace target domain. We remark that these preserved concepts are useful to the target domain (Palace) for adaptation.

Limitations of GAN Dissection / Future Work : Although GAN Dissection can uncover useful semantic concepts preserved by high FI kernels, GAN Dissection method [45] is limited by the dataset used for semantic segmentation. Hence this method is not able to uncover concepts that are not present in semantic segmentation dataset (They use Broaden Dataset [46]). Therefore, using GAN dissection we are currently unable to discover and visualize more fine-grained concepts preserved by our high FI kernels. We hope to further address this problem in future work.

12 Main Paper Experiments : Additional Results / Analysis

12.1 KID / Intra-LPIPS / Standard Deviation of Experiments

KID / Intra-LPIPS. In addition to FID scores reported in the main paper, we evaluate KID [66] and Intra-LPIPS [38]. We remark the KID (\downarrow) is another metric in addition to FID (\downarrow) to measure the quality of generated samples, and Intra-LPIPS (\uparrow) measures the diversity of generated samples. In literature, the original LPIPS [38] evaluates the perceptual distance between images. We follow CDC [14] and DCL [19] to measure the Intra-LPIPS, a variant of LPIPS, to evaluate the degree of diversity. Firstly, we generate 5,000 images and assign them to one of 10-shot target samples, based on the closet LPIPS distance. Then, we calculate the LPIPS of 10 clusters and take average. KID and

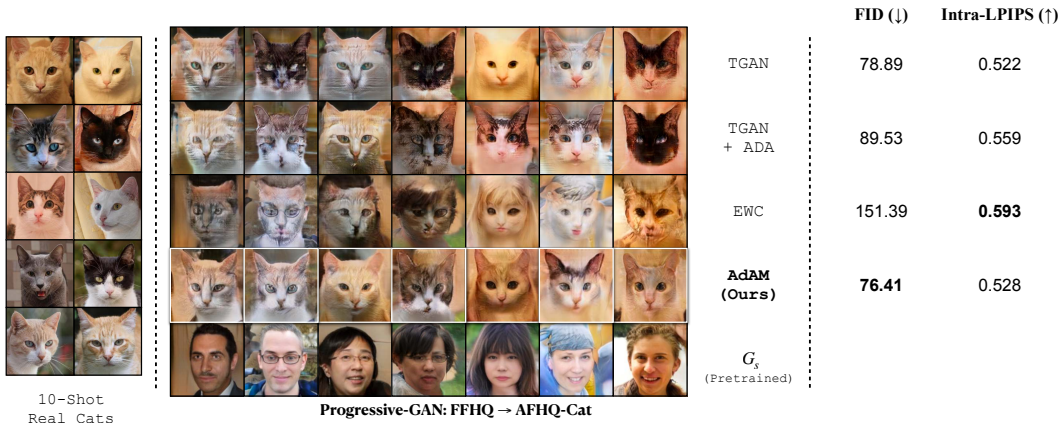


Figure 14: FFHQ → Cat 10-shot adaptation results using pre-trained ProGAN [64] generator. We include ADA results. As one can observe, our proposed method outperforms existing FSIG methods.

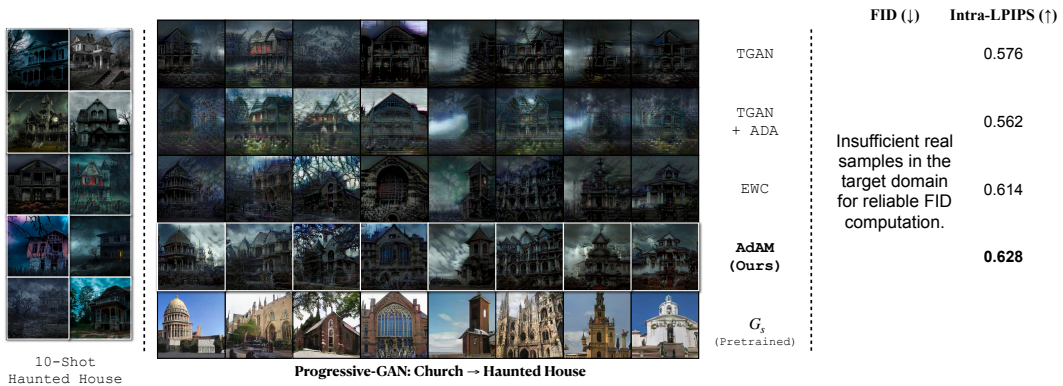


Figure 15: Church → Haunted Houses 10-shot adaptation results using pre-trained ProGAN [64] generator. We include ADA results.

Intra-LPIPS results are reported in Tables 6 and 7 respectively. As one can observe, our proposed adaptation-aware FSIG method outperforms SOTA FSIG methods [18, 14, 19] and produces high quality images with good diversity.

Table 6: KID (↓) score of different methods with the same checkpoint of Table 2 in the main paper. The values are in 10^3 units, following [36, 12].

Method	TGAN	FreezeD	EWC	CDC	DCL	AdAM (Ours)
Babies	81.92	65.14	51.81	51.74	43.46	28.38
AFHQ-Cat	41.912	38.834	58.65	196.60	117.82	32.78

Table 7: Intra-LPIPS (↑) of different methods, the standard deviation is calculated over 10 clusters. Compared to the baseline models (TGAN/FreezeD) or state-of-the-art FSIG methods (EWC/CDC/DCL), our proposed method can achieve a good trade-off between diversity and quality of the generated images, see Table 2 in main paper for FID score.

Method	TGAN	FreezeD	EWC	CDC	DCL	AdAM (Ours)
Babies	0.517 ± 0.04	0.518 ± 0.05	0.521 ± 0.03	0.578 ± 0.03	0.580 ± 0.02	0.590 ± 0.03
AFHQ-Cat	0.490 ± 0.02	0.492 ± 0.04	0.587 ± 0.04	0.629 ± 0.03	0.616 ± 0.05	0.557 ± 0.02

Standard Deviation of FID scores. We report standard deviation of FID scores for Babies and Cat corresponding to the main paper experiments (Table 2: main paper) in Table 8. As one can observe, the standard deviations are within acceptable range.

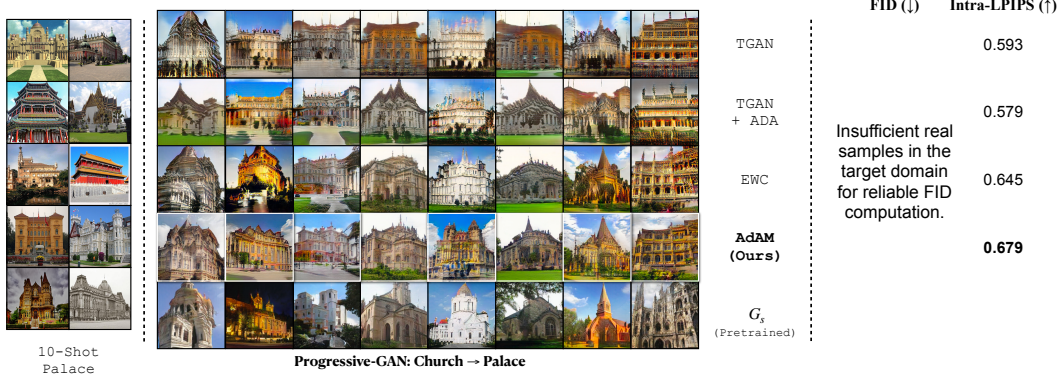


Figure 16: Church \rightarrow Palace 10-shot adaptation results using pre-trained ProGAN [64] generator. We include ADA results.

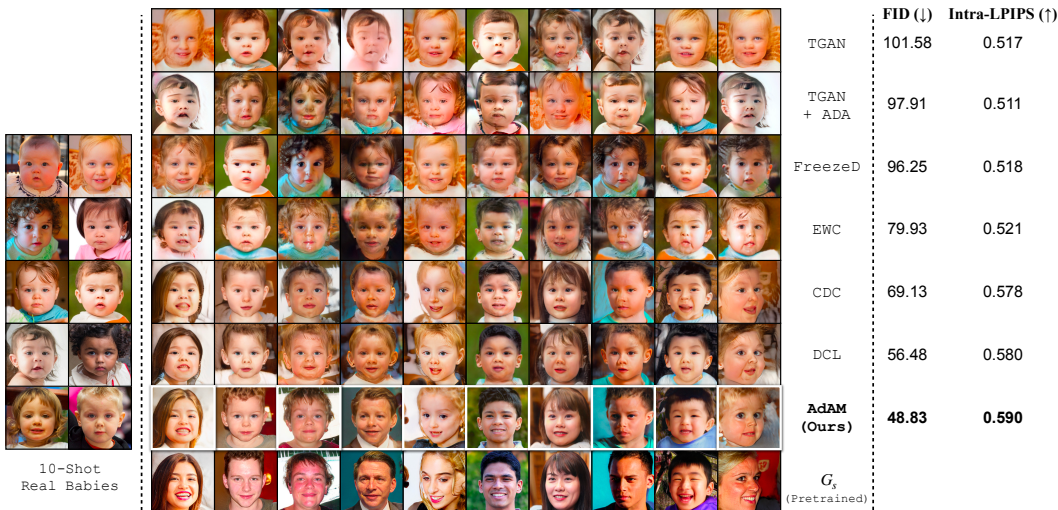


Figure 17: FFHQ \rightarrow Babies results, including ADA [36].

Table 8: FID score (\downarrow) with standard deviation over 3 different runs.

Method	TGAN	FreezeD	EWC	CDC	DCL	AdAM (Ours)
Babies	101.69 \pm 0.50	97.15 \pm 1.02	79.59 \pm 0.26	66.98 \pm 1.58	56.64 \pm 0.90	47.92 \pm 0.87
AFHQ-Cat	64.60 \pm 0.68	64.56 \pm 0.69	74.69 \pm 0.32	174.5 \pm 2.55	154.60 \pm 1.98	57.59 \pm 0.36

12.2 10-shot Adaptation Results

We show complete 10-shot adaptation results for our proposed adaptation-aware FSIG method and existing FSIG methods [16, 18, 14, 19] for distant target domains. Results for FFHQ \rightarrow Dog and FFHQ \rightarrow Wild are shown in Figures 22 and 23 respectively. As one can observe, SOTA FSIG methods [18, 14, 19] are unable to adapt well to distant target domains (palace, yurt) due to *due to only considering source domain / task in knowledge preservation*. We remark that TGAN [16] suffers severe mode collapse. We clearly show that our proposed adaptation-aware FSIG method outperforms SOTA FSIG methods [18, 14, 19] and produces high quality images with good diversity.

We further show 10-shot adaptation results for our proposed adaptation-aware FSIG method for additional setups. We show 10-shot adaptation results for FFHQ \rightarrow MetFaces [36] (Figure 26), FFHQ \rightarrow Sketches (Figure 27), FFHQ \rightarrow Sunglasses (Figure 25), FFHQ \rightarrow Amedeo Modigliani’s Paintings (Figure 28), FFHQ \rightarrow Otto Dix’s Paintings (29) and Cars \rightarrow Wrecked Cars (Figure 31).

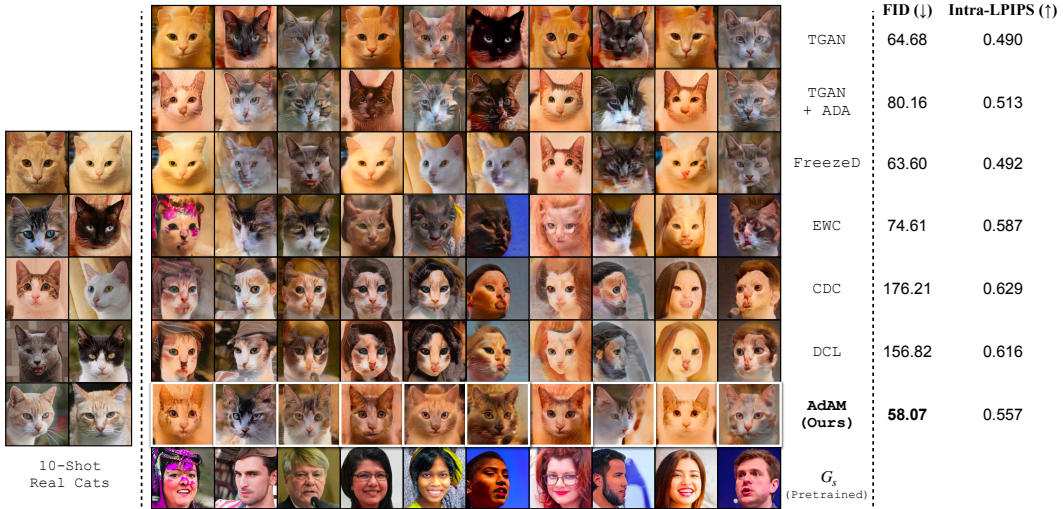


Figure 18: FFHQ → Babies results, including ADA [36].

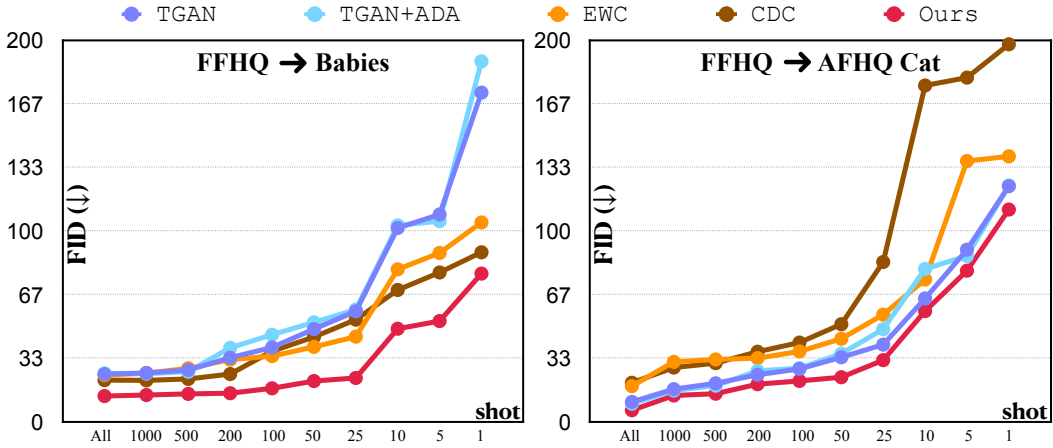


Figure 19: We add more data points based on Figure 6 in the main paper, and conduct experiments given extremely limited number of samples. We also include the entire dataset for adaptation.

12.3 100-shot adaptation

In addition to the analysis of increasing the number of shots for target adaptation in Figure 6 of main paper, here we additionally show the generated images with 100-shot training data, on Babies and AFHQ-Cat. The results are shown in Figure 32 where each column represents a fixed noise. Compared to baseline and SOTA methods, our generated images can still produce the best quality and diversity.

12.4 FID measurements with limited target domain samples

To characterize source → target domain proximity, we used FID and LPIPS measurements. FID involves distribution estimation using first-order (mean) and second-order (trace) moments, i.e.: $FID = mean_{component} + trace_{component}$ [44] Generally, 50K real and generated samples are used for FID calculation³. Given that our target domain datasets contain limited samples, i.e.: Cat [5], Dog [5], Wild [5] datasets contain $\approx 5K$ samples, we conduct extensive experiments to show that FID measurements with limited samples give reliable estimates, thereby reliably characterizing source

³Chong, Min Jin, and David Forsyth. "Effectively unbiased fid and inception score and where to find them." Proceedings of the IEEE/CVF conference on computer vision and pattern recognition. 2020.

Visualizing the Importance Probing Results using GAN Dissection

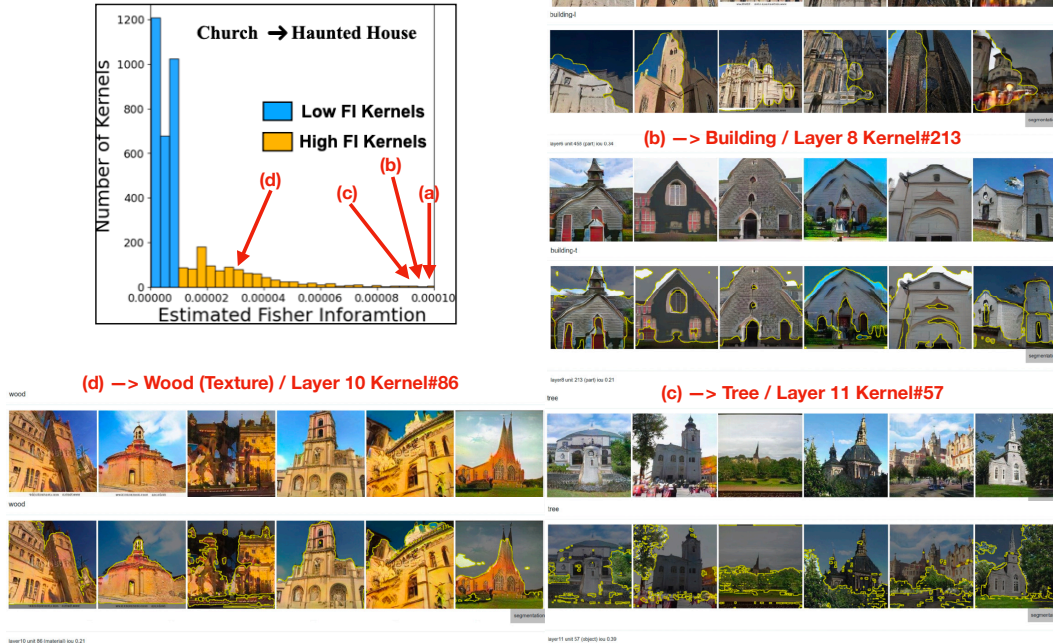


Figure 20: Visualizing high FI kernels using GAN Dissection [45] for Church → Haunted Houses 10-shot adaptation. In visualization of each high FI kernel, the first row shows different images generated by the source generator, and the second row highlights the concept encoded by the corresponding high FI kernel as determined by GAN Dissection. We observe that a notable amount of high FI kernels correspond to useful source domain concepts including building (a, b), tree (c) and wood (d) which are preserved when adapting to Haunted Houses target domain. We remark that these preserved concepts are useful to the target domain (Haunted House) for adaptation.

→ target domain proximity. Specifically, we decompose FID into mean and trace components and study the effect of target domain sample size to show that our proximity measurements using FID are reliable.

Experiment Setup. We use 3 large datasets namely FFHQ [3] (70K samples), LSUN-Bedroom [67] (70K samples) and LSUN-Cat [67] (70K samples). We use FFHQ (70K samples) as the source domain and study the effect of sample size on FID measure. Specifically, we decompose FID into mean and trace components in this study. We consider FFHQ (self-measurement), LSUN-Bedroom and LSUN-cat as target domains. We sample 13, 130, 1300, 2600, 5200, 13000, 52000 samples from the target domain and measure the FID with FFHQ (70K samples), and compare it against the FID obtained by using the entire 70K samples from the target domain.

Results / Analysis. The results are shown in Table 9. As one can observe, with ≈ 2600 samples, we can reliably estimate FID as it becomes closer to the FID measured using the entire 70K target domain samples. Hence, we show that our source → target proximity measurements using FID are reliable.

13 Discussion: How much can the proximity between source and target be relaxed?

In this section, we explore the proximity limitation between source and target domains in our experiment setups. First, we remark that the upper bound on proximity between the source domain S

Visualizing the Importance Probing Results using GAN Dissection

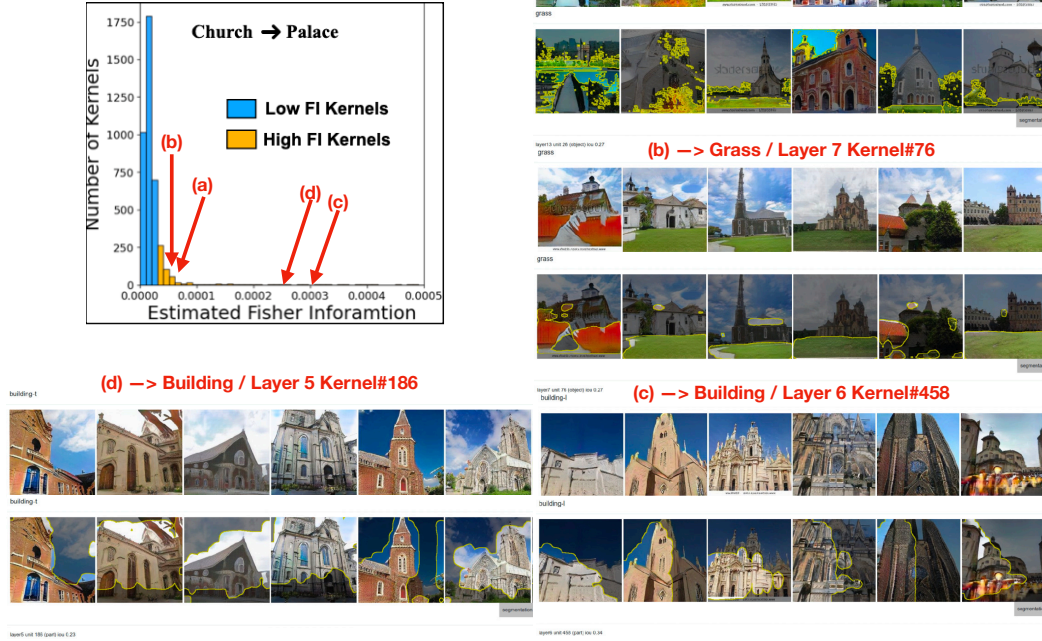


Figure 21: Visualizing high FI kernels using GAN Dissection [45] for Church → Palace 10-shot adaptation. In visualization of each high FI kernel, the first row shows different images generated by the source generator, and the second row highlights the concept encoded by the corresponding high FI kernel as determined by GAN Dissection. We observe that a notable amount of high FI kernels correspond to useful source domain concepts including grass (a, b) and building (c, d) which are preserved when adapting to Palace target domain. We remark that these preserved concepts are useful to the target domain (palace) for adaptation.



Figure 22: FFHQ → AFHQ-Dog (distant domain)

and the target domain T could be conditioning on (a) the number of available samples (shots) from the target domain, and (b) the method used for knowledge transfer.

(a) Proximity bound conditioning on the number of target domain samples. In this paper, we focus on few-shot setups, e.g. 10 shots. However, with more target domain samples available, proximity between S and T can be further relaxed, and the proximity bound would increase, i.e. for a given generative model on S , we could learn an adapted model for T which is more distant. Intuitively, increasing the number of target domain samples can provide more diverse knowledge for T , and as a result, there is less reliance on the knowledge of S that is generalizable for T (which would decrease



Figure 23: FFHQ → AFHQ-Wild (distant domain)

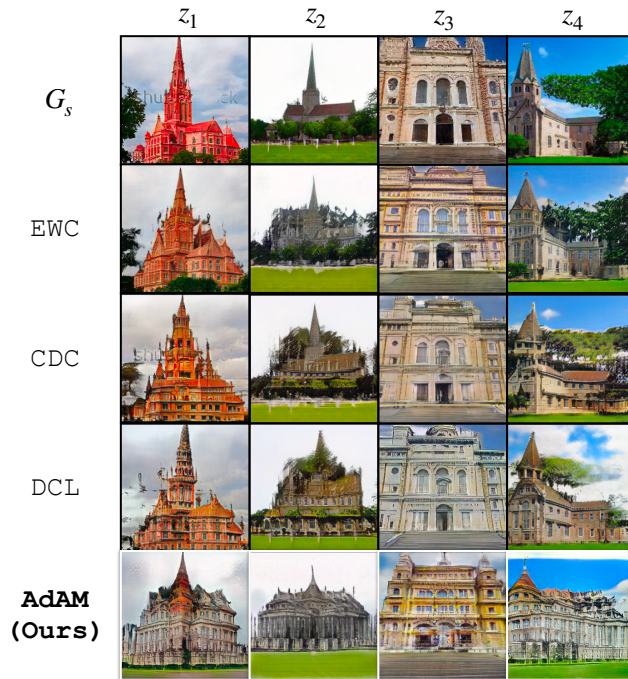


Figure 24: Church → Palace (distant domain)

as S and T are more apart). In the limiting cases when abundant target domain samples are available, knowledge of S would not be critical, and proximity constraints between S and T may be totally relaxed (ignored).

(b) Proximity bound conditioning on the knowledge transfer method. Given a generative model pretrained on S and a certain number of available samples from T , the method used for knowledge transfer plays a critical role. If the method is superior in identifying suitable transferable knowledge from S to T , the proximity between S and T can be relaxed, and the proximity bound would increase. In our work, our first contribution is to reveal that existing SOTA approaches (which are based on target-agnostic ideas) are inadequate in identifying transferable knowledge from S to T . As a result, when proximity between S and T is relaxed, the performance of the adapted models is miserably poor, as discussed in Sec.3, Sec.5, and Appendix. Therefore, our second contribution is to propose a target-aware approach that could identify more meaningful transferable knowledge from S to T , allowing relaxation of the proximity constraint.

In this section, we provide experimental results for the adaptation between two very distant domains: FFHQ→Cars using only 10-shots, aiming to answer two main questions: (1) Is there transferable knowledge from FFHQ to Cars for the FSIG task? (2) How does our proposed method compare with

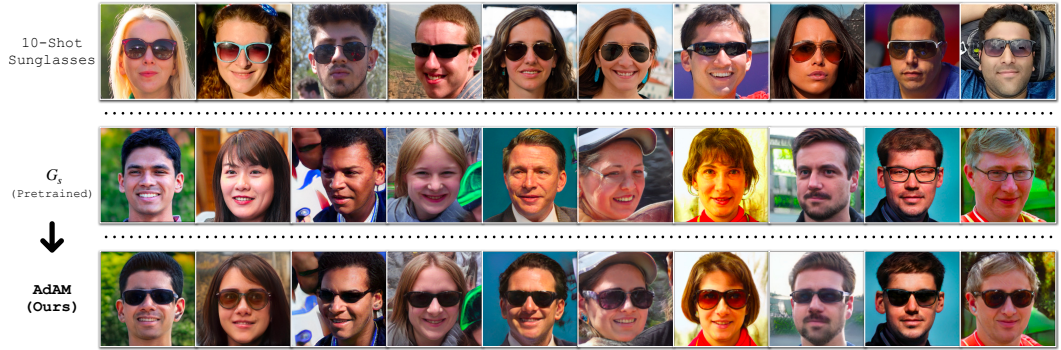


Figure 25: FFHQ → Sunglasses



Figure 26: FFHQ → MetFaces



Figure 27: FFHQ → Sketches



Figure 28: FFHQ → Amedeo Modigliani's Paintings



Figure 29: FFHQ → Otto Dix's Paintings



Figure 30: FFHQ → Raphael's Paintings



Figure 31: Cars → Wrecked Cars

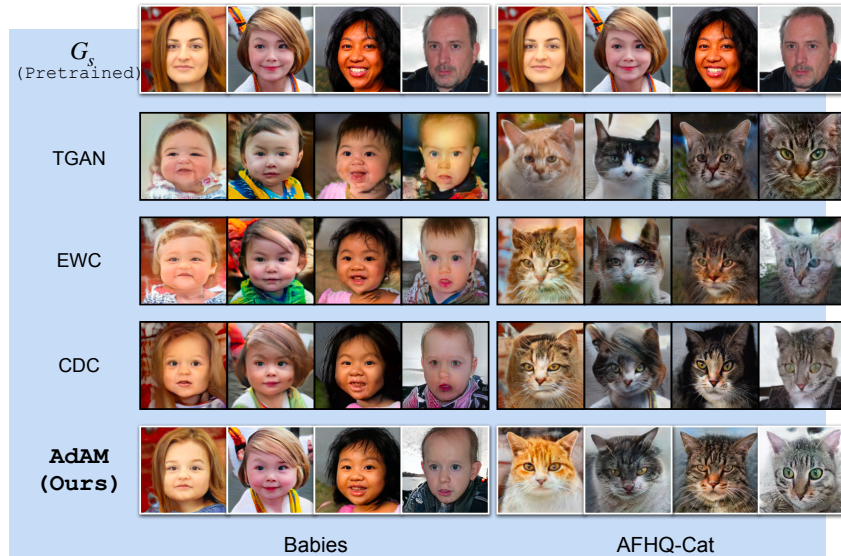


Figure 32: FFHQ \rightarrow Babies (Left) and AFHQ-Cat (Right) with 100 samples for adaptation.

Table 9: *FID measurements with limited target domain samples give reliable estimates to characterize source \rightarrow target domain proximity*: FFHQ (70K) is the source domain. We use FFHQ (self-measurement), LSUN-Bedroom and LSUN-Cat as target domains. We use different number of samples from target domain to measure FID. We also decompose FID into mean and trace components in this study. We sample 13, 130, 1300, 2600, 5200, 13000, 52000 images from the target domain and measure the FID with source domain (FFHQ / 70K), and compare it against the FID obtained by using the entire 70K samples from the target domain. Each experiment is repeated *100 times* and we report the results with standard deviation. We also report mean and trace components separately. As one can observe, with ≈ 2600 samples, we can reliably estimate FID as it becomes closer to the FID measured using the entire 70K target domain samples. Therefore, this study shows that our source \rightarrow target proximity measurements using FID are reliable.

FID		13	130	1300	2600	5200	13,000	52,000	70,000
FFHQ	FID	196.3 \pm 11.8	83.4 \pm 2.2	15.3 \pm 0.2	7 \pm 0.1	3.3 \pm 0	1.2 \pm 0	0.1 \pm 0	0 \pm 0
	mean	12 \pm 2.7	1.3 \pm 0.3	0.1 \pm 0	0.1 \pm 0	0 \pm 0	0 \pm 0	0 \pm 0	0 \pm 0
	trace	184.3 \pm 10.3	82.2 \pm 2	15.2 \pm 0.2	6.9 \pm 0.1	3.3 \pm 0	1.1 \pm 0	0.1 \pm 0	0 \pm 0
Bedroom	FID	358.5 \pm 9.3	301.9 \pm 2.4	251 \pm 1.2	243.6 \pm 0.8	240.1 \pm 0.5	238.2 \pm 0.4	237.2 \pm 0.2	237.2 \pm 0.1
	mean	139.3 \pm 8	131.8 \pm 2.5	131.4 \pm 0.9	131.1 \pm 0.6	131.1 \pm 0.4	131.1 \pm 0.3	131.1 \pm 0.1	131.1 \pm 0.1
	trace	219.1 \pm 9.9	170.1 \pm 1.9	119.6 \pm 0.6	112.5 \pm 0.4	109.1 \pm 0.3	107.1 \pm 0.2	106.1 \pm 0.1	106 \pm 0.1
Cat	FID	370.2 \pm 18.7	283.7 \pm 4.4	209.7 \pm 1.2	199.9 \pm 0.8	195.3 \pm 0.6	192.8 \pm 0.4	191.4 \pm 0.2	191.3 \pm 0.1
	mean	105.7 \pm 8.4	93 \pm 2.2	91.7 \pm 0.8	91.7 \pm 0.5	91.6 \pm 0.4	91.6 \pm 0.2	91.6 \pm 0.1	91.6 \pm 0.1
	trace	264.5 \pm 15.7	190.7 \pm 3.6	118 \pm 0.9	108.2 \pm 0.6	103.7 \pm 0.4	101.2 \pm 0.3	99.9 \pm 0.1	99.7 \pm 0.1

other methods in this setup? For this, in addition to transfer learning approaches discussed in the paper, we also add the results for training from scratch using only the same 10 Car samples. The quantitative results are in Table 10.

The results suggest that even though domain FFHQ and domain Cars are apart, there is still useful and transferable knowledge from FFHQ to Cars (e.g. low-level edges, shapes), leading to better performance (FID, Intra-LPIPS) in the adapted model using proposed method compared to the one which is trained from scratch. In addition, our proposed method can identify and transfer more meaningful knowledge compared to other baselines and SOTA methods, resulting in lower FID and higher diversity in generated images.

Table 10: We conduct experiments for FFHQ \rightarrow Cars adaptation and evaluate the performance in such a challenging setup. We show that our method can achieve similar diversity as ADA [36] and the overall performance (FID) is better than other baseline and SOTA methods.

Domain	FFHQ \rightarrow Cars	
	FID (\downarrow)	Intra-LPIPS (\uparrow)
Train from Scratch	201.34	0.300
ADA [36]	171.98	0.438
EWC [18]	276.19	0.620
CDC [14]	109.53	0.484
DCL [19]	125.96	0.464
AdAM (Ours)	80.55	0.425

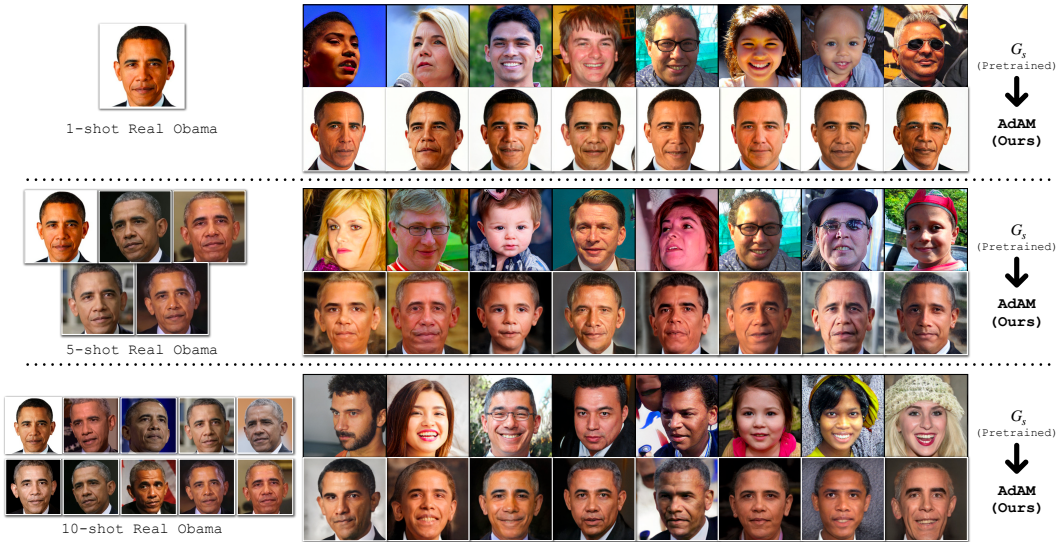


Figure 33: FFHQ \rightarrow Obama Dataset

14 Additional information for Checklist

14.1 Potential Societal Impact

Given very limited target domain samples (i.e.: 10-shot), our proposed method achieves SOTA results in FSIG with different source / target domain proximity. Though our work shows exciting results by pushing the limits of FSIG, we urge researchers, practitioners and developers to use our work with privacy, ethical and moral concerns. In what next, we bring an example to our discussion.

Adapting the pretrained GAN to a particular person. The idea of FSIG aims to adapt a pretrained GAN to a target domain with limited samples. It is reasonable that a user of FSIG can take few-shot images of a particular person and generate diverse images of the person, which leads to potential safety and privacy concerns. We conduct an experiment to adapt a pretrained StyleGAN2 generator to Obama dataset [68] in 1-shot, 5-shot and 10-shot setups, and the results are shown in 33.

Potentially, the method can be adapted to generate images of the same person by applying a more restrictive selection of the source model’s knowledge. However, this would degrade the diversity of the outputs and may not be suitable for general FSIG which our paper focuses on. We will explore such interesting application as our future work and verify with state-of-the-art face recognition systems to understand any potential threats.

14.2 Amount of Compute

The amount of compute in this project is reported in Table 11. We follow NeurIPS guidelines to include the amount of compute for different experiments along with CO_2 emission.

Table 11: Amount of compute in this project. The GPU hours include computations for initial explorations / experiments to produce the reported values. CO_2 emission values are computed using <https://mlco2.github.io/impact/>

Experiment	Hardware	GPU hours	Carbon emitted in kg
Main paper : Table 2 (Repeated 3 times)	Tesla V100-PCIE (32 GB)	306	52.33
Main paper : Figure 5 / Figure 6	Tesla V100-PCIE (32 GB)	136	23.26
Main paper : Figure 2	Tesla V100-PCIE (32 GB)	6	1.03
Supplementary : Extended Experiments	Tesla V100-PCIE (32 GB)	68	11.63
Supplementary : Ablation Study	Tesla V100-PCIE (32 GB)	14	4.1
Additional Compute for Hyper-parameter tuning	Tesla V100-PCIE (32 GB)	24	2.16
Total		554	94.73